Finite Element Analyses and Proposed Strengthening of a Reinforced Concrete Box Girder Bridge Subjected to Differential Settlement

by

Caleb Mitchell

B.S., Kansas State University, 2016

A THESIS

submitted in partial fulfillment of the requirements for the degree

MASTER OF SCIENCE

Department of Civil Engineering
College of Engineering

KANSAS STATE UNIVERSITY
Manhattan, Kansas

2018

Approved by:

Major Professor
Dr. Hayder A. Rasheed

Copyright

Abstract

The Kansas Department of Transportation's (KDOT) Bridge 059-045 is a reinforced concrete box girder bridge constructed in 1965 to connect the rural Shawnee Drive across Interstate 135 near McPhearson, Kansas, in between Salina and Wichita. The bridge was observed, during an annual inspection in 1998, to have experienced some settlement, which was further found to be due to its proximity to a sinkhole. This settlement progressed to noticeable levels in 2012 necessitating a semi-annual elevation profile survey that was consistently conducted by KDOT. In April 2016, KDOT determined that the bridge required a detailed finite element analysis to determine the safety and suitability of the bridge to stay open to traffic. Accordingly, a two-level Finite Element Analysis was performed using RISA 3D and Abaqus to assess the level of distress in the bridge due to the continuous differential settlement as a result of the active sinkhole deep in the soil under the bridge. The force-moment results were taken from the RISA 3D model for further analysis of various structural components that make up the bridge, including the box girder, piers, and piles. The stress distribution results from the Abaqus model were investigated for the same components of the bridge. A strengthening design scheme using near surface mounted fiber reinforced polymer rebar was developed to extend the service life of the bridge.

Table of Contents

List of Figures

List of Tables

Acknowledgements

I would like to thank my advisor, Dr. Hayder Rasheed, for giving me the opportunity to work on this project and giving me guidance on the project and my academics. I would also like to thank Dr. Hani Melhem and Dr. Christopher Jones for serving on my advisory committee.

Thanks to Mark Hoppe, Jon Jones, Jon Waller, Steve Burnett and everyone else in the Kansas Department of Transportation's Bureau of Structural and Geotechnical Services for sponsoring this project and providing the data necessary to complete it.

Thank you to Dr. Habiburrahman Ahmadi and Jack Olson for assisting with the modeling portions of the project.

Introduction

Geological formations in terms of salt sinkholes exist in deep soil strata in Kansas. This problem is a challenging issue for transportation infrastructure, especially bridges. Even though deep foundations are typically implemented, super structures suffer from slow rates of settlements inducing seriously large stresses particularly in statically indeterminate bridges. These induced stresses often build up to reach the maximum limits of member envelopes which may lead to compromising safety by promoting the attainment of strength limit states.

Unexpected settlement is a common issue that has to be dealt with across the country. Past drilling and mining can create voids in the Earth that can be unaccounted for during initial design of a highway or bridge. The same phenomenon that caused the sinkhole, at this bridge site, caused three separate sinkholes along I-70 in Russell County, Kansas. At these locations, the Kansas Department of Transportation (KDOT) has attempted to slow the settlement down by placing soil and concrete into the sinkholes, but settlement continues to occur at these locations. A county bridge at the Russell County location, was forced to be torn down after it settled nearly six feet (Dedo, 2017). Many other examples of this occur across the country due to previous activity that was not regulated at the turn of the 20th century. A large number of mines were not considered in the design process because their operations ended before the Bureau of Mines began to require maps of where the mines were located (Lefchik, Ruegsegger, and Henthorne, 2003). There are many techniques that are used to identify where these voids are today, but they are often only used on new construction or after settlement has been noticed around an existing structure. These methods are often nondestructive, which allows for testing around existing structures without causing any more damage to the affected area. These tests often include seismic refraction and reflection, where the wave velocity depends on the type of material the wave passes through, and ground penetrating radar which uses the reflection of radio waves to electromagnetic frequencies in materials of varying dielectric permittivity (Armstrong, Surdahl, and Armstrong, 2009). These tests are able to map voids and determine an accurate map of what lies beneath the surface, but have high costs that many state

Departments of Transportation do not have the money to fund, which results in the use of destructive tests such as borings being used to map the affected area. The main problem that results from finding these voids is what to do after they have been identified. The most common practice is to try and pump various materials, such as concrete or grout, into the sinkhole to dry and strengthen the area. At the sinkhole in Russel County, KDOT has spent more than three million dollars in projects to attempt to fill in the sinkholes with the settlement still continuing today (Dedo, 2017).

Background and Objectives

The settlement at this location has been possibly occurring since the bridge was built. KDOT believes that the settlement is caused by abandoned oil wells in the area. In the 1920s there were few regulations on oil production, which led to rapid withdrawals from the areas. The wells were drilled through many layers in order to reach the oil, which included sandstone, groundwater, shale, and thick salt deposits. The oil was removed rapidly which caused the sites to run out of oil and then be abandoned. According to KDOT Regional Geologist Neil Croxton, "Whatever plugging was done, if anything was done, was not successful" (Dedo, 2017). The ineffective plugging allowed for the ground water to get past the shale, which protects the salt layer from the water. The water then dissolved the salt layer, which created voids underground and lead to gradual settlement over time.

When the bridge was built in 1965, nine borings were taken around the location of the bridge. These were used to determine the soil conditions under the bridge in order to design the depth of the piles and to find depth of the bedrock. In 2017, 23 borings were taken to determine how the soil layers and the depth of the bedrock had changed since the bridge was originally built. Figure 1 shows the drop in bedrock elevation from 1965 to 2017.

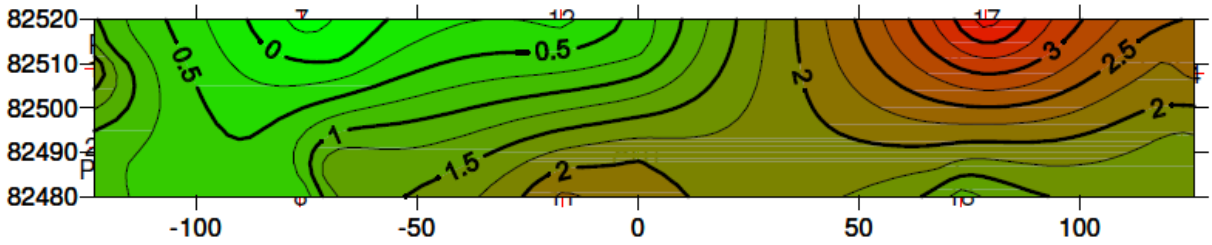

Figure 1: Drop in Bedrock Elevation Below Bridge (Feet), Courtesy of KDOT Bureau of Structural and Geotechnical Services

The drop in bedrock ranges from zero feet on the west side of the bridge to over three feet on the east side. This drop in the bedrock shows how the settlement of the bridge was able to take place over time, but it is not an accurate measurement of how the bridge itself is settling. Starting in 2012, survey crews from KDOT have taken survey shots of the bridge to determine how it has settled from its original state. The change in elevation of the bedrock provides a good guide as to what the bridge settlements are, but are not exact. There is no change in bedrock elevation at abutment 1 and there is no settlement at abutment 1 according to the survey data, but this exact correlation is not always the case. The change in bedrock elevation would suggest that the highest settlement values would be on the north side of the bridge at pier 3 and abutment 2, while in reality the largest settlement values are at pier 2 and pier 3 on the south side of the bridge. The Figure 2 shows the settlement profile of the bridge in April of 2017.

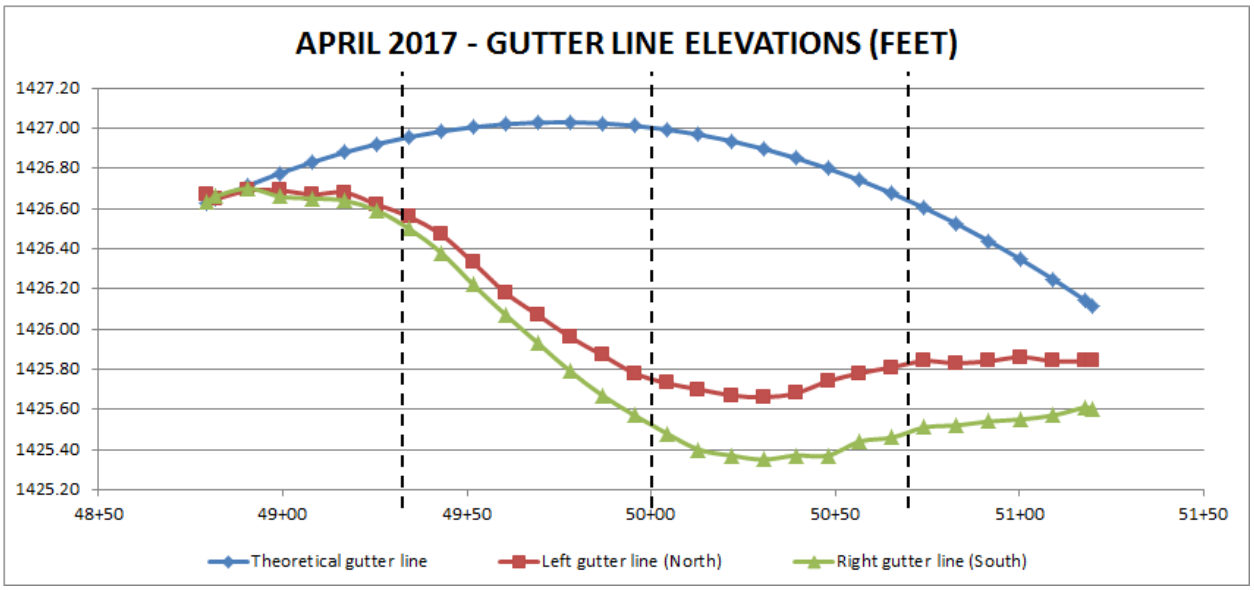

Figure 2: April 2017 Settlement Profile

The profile shows the theoretical gutter line of the bridge when it was originally built, along with the actual gutter line of the bridge on the south and north side of the bridge. The lines begin at abutment one on the west side of the bridge and ends at abutment 2 on the east side of the bridge. The three dashed lines on the graph represent the locations on the piers. Pier 1 is closest to abutment 1, then pier 2 in the middle, and pier 3 is closest to abutment 2. The south side of the bridge settles more than the north side of the bridge, which creates torsion in the box girder of the bridge along with the bending due to the settlement. The maximum settlement values occur in the middle of pier 2 and pier 3. Figures 3 and 4 show the elevation and plan view of the bridge.

Figure 3: Elevation View

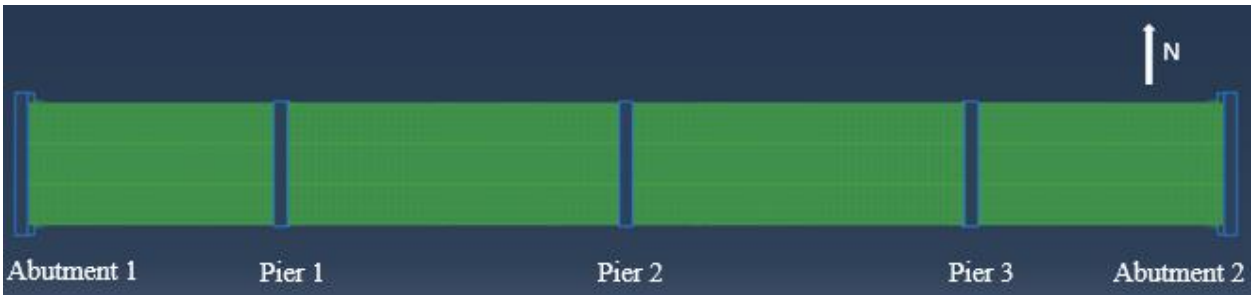

Figure 4: Plan View

The settlements at each location are shown in Table 1.

Table 1: Total Settlements in April 2017

April 2017 Total Settlements		
	South (in.)	North (in.)
Abutment 1	0	0
Pier 1	-5.21	-4.65
Pier 2	-17.80	-15.10
Pier 3	-14.27	-10.21
Abutment 2	-6.38	-3.62

These settlement values have led to the objectives of this study. These objectives include:

1. Perform a detailed 3D finite element analysis of the bridge using Abaqus to assess the levels of stresses in the various structural components of the bridge.

2. Perform a detailed 3D finite element analysis of the bridge using RISA 3D to assess the forces and moments obtained at various structural components and to plot them against section envelope curves.

3. Propose schemes to strengthen the bridge structural components using FRP to extend its life span, if this is found to be an effective solution.

4. Monitor the long term settlement of the bridge for five years if the bridge was deemed stable and safe to be kept open to traffic.

Finite Element Modeling

Geometric Properties

The overall length of the bridge is 240 feet and 8 inches, with spans 2 and 3 being 68 feet and spans 1 and 4 being 51 feet. Each span is made up of an identical box girder, which has an overall depth of 4 feet. The box girder is separated into three sections, with each of the boxes having a width of 8 feet 2 inches center to center. The top of the box girder is made of a 7 inch uniform slab. The flexural reinforcement pattern in the top slab near the pier is made up of two layers of steel, where the spacing and size varies throughout each span. The bottom of the box girder is made of a 6 inch uniform slab. The flexural reinforcement pattern in the bottom slab near the pier is a single layer of steel made of #8 bars with various spacing. The webs in the box girder have a 9 inch width at the pier and then taper to an 8 inch width at mid-span. The flexural reinforcement remains constant throughout the pier, which consists of 2 #8 bars at top of the web, 2 #5 bars at mid-height, and 2 #5 bars at the bottom of the web. #4 bars are used as stirrups in the web. Figure 5 shows a cross section of the box girder that was described above.

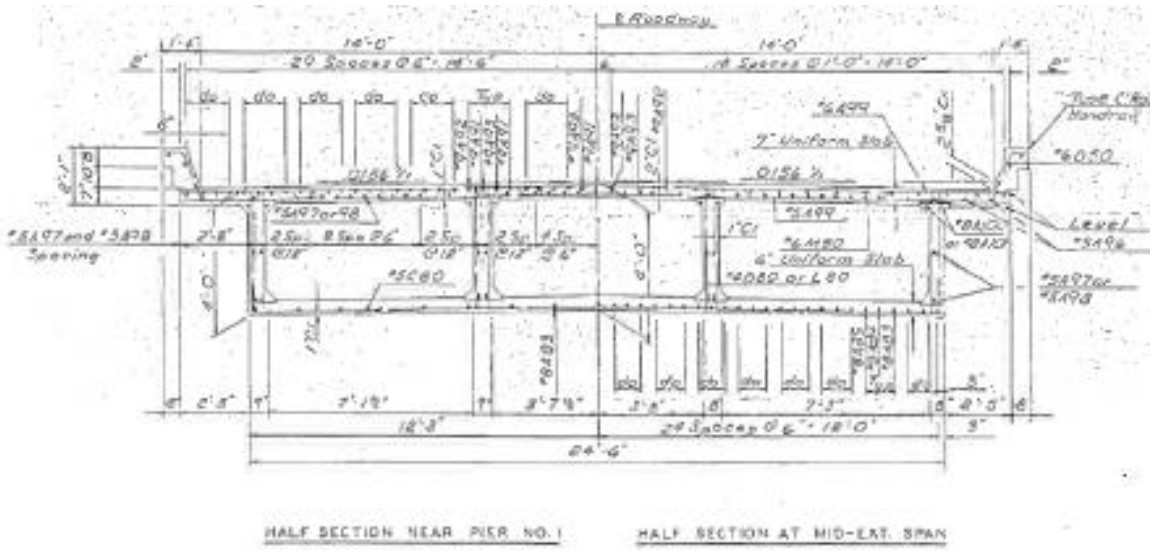

Figure 5: Cross Section of Box Girder, Courtesy of KDOT Bureau of Structural and Geotechnical Services

At each pier, a 2 foot 8 inch wide solid concrete cross beam connects each span together. The cross beam is reinforced with 7 #10 bars at the top and bottom of the section and are tied together with #5 stirrups at various spacing across the beam. The solid cross beams allow for the load from the box girder to be effectively transferred to the piers. There are two piers at each cross beam that are circular with a 2 foot 6 inch diameter. The piers are reinforced with 9 #8 bars that are tied together with 3/8 inch spiral reinforcement at a 6 inch pitch spacing. Each pier is supported by a 5-foot square pile cap that is 3 feet in thickness. The pile cap is reinforced by a two layer reinforcement mesh consisting of #6 bars spaced at 6 inches in each direction. There are four piles used to support each pier. The piles are 12BP53, which are an H-pile shape that is no longer in production. The pile cross section has a depth and width of 12 inches, are imbedded 1 foot into the pile cap and extend 15 feet into the ground. Figure 6 presents the cross beam, pier, and pile cap dimensions that were described above.

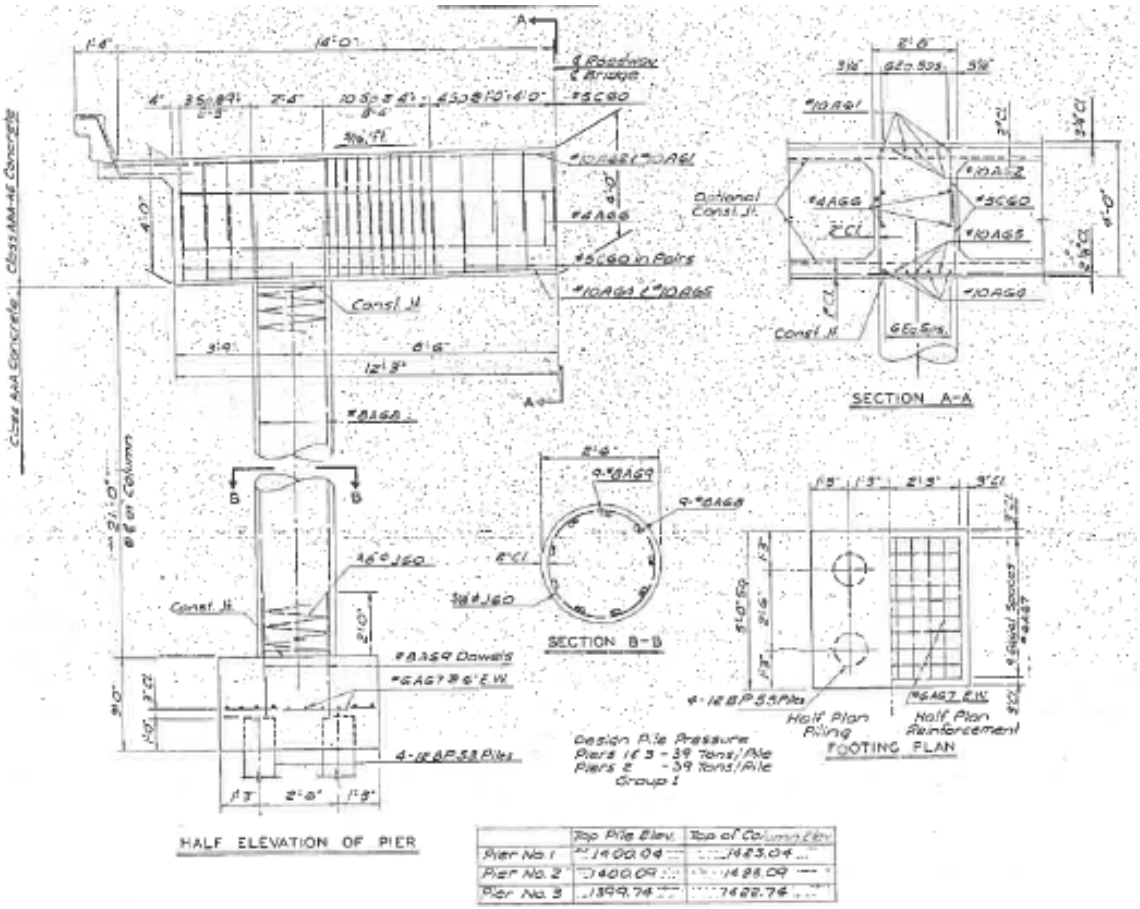

Figure 6: Cross Beam, Pier, and Pile Cap Dimensions, Courtesy of KDOT Bureau of Structural and Geotechnical Services

At either end of the bridge, there is a 2 foot 6 inch rectangular abutment that has a depth of 7 feet. The abutments are supported by 5 10BP42 piles that are spaced evenly across the abutment. The piles are an H-pile shape that has a depth of 10 inches and a width of 10 inches. The piles are imbedded 1 foot 6 inches into the abutment and extend to a depth of 41 feet under the west abutment and 36 feet under the east abutment.

Material Properties

When creating each model, the elastic modulus of concrete was taken to be 33% of the original modulus of concrete for a concrete with a compressive strength of 4000 psi. The original modulus was found by taking 57000 times the square root of the compressive strength. This was done to account for the cracking in the concrete as well as the creep that the concrete has experienced since it was placed in situ. The moment of inertia of cracked concrete is approximately half that of the gross moment of inertia. Cracking was observed during the site inspection and through calculations of the effective tensile stresses in the elements exceeding the modulus of rupture of concrete. Figures 7 and 8 show examples of cracking that was observed in the bridge.

Figure 7: Shear Crack in Web of Box Girder

Figure 8: Radial Cracks at Top of Pier

Since the geometry considered was the original unchanged dimensions, cracking was accounted for by reducing the modulus of elasticity to 50% of its initial value which is equivalent to reducing the moment of inertia by such a reduction factor. Then to account for the long term creep of the concrete, the elastic modulus was further reduced to 33% of the original value, as per the practice of KDOT bridge design engineers. This value is important when the finite element models determine the stiffness in each element while running the analysis. By lowering the stiffness values of the elements, the bridge is able to have more flexibility and is able to deform similar to the bridge's current conditions. Since the lower stiffness allows the model to deform similar to how the bridge is deforming on site, the forces and stresses experienced in the elements are anticipated to be similar to those experienced in the bridge. Furthermore, the Poisson ratio of the cracked concrete is assumed to be 0.2. In each model the concrete components were modeled without the steel reinforcement.

The piles that support the bridge were modeled with lateral springs acting in the x and z directions, to brace the piles like the soils that surrounds them. The coefficients of the springs were determined by the following equations.

$$K_s(kcf) = 250 + 125\sqrt{Y(ft)} \quad \text{Equation 1}$$

$$K_1(kpf) = H * B * \frac{2K_{S1}+K_{S2}}{6} \quad \text{Equation 2}$$

$$K_2(kpf) = \begin{cases} K'_{21} = H * B * \frac{2*K_{S2}+K_{S1}}{6} \\ K'_{22} = H * B * \frac{2*K_{S2}+K_{S3}}{6} \end{cases} = K'_{21} + K'_{22} \quad \text{Equation 3}$$

$$K_N(kpf) = H * B * \frac{2K_{SN}+K_{SN-1}}{6} \quad \text{Equation 4}$$

In Equation 1, the lateral stiffness in kips per cubic foot is found by adapting the coefficients estimated by Bowles 1996 for a comparable soil. In Equations 2-4, the lateral stiffness in kips per linear foot is calculated by multiplying by the tributary area (the depth between the two points (H), the width of the pile (B), by twice the coefficient at that depth plus the coefficient at the depth at the point above divided by 6) (Bowles, 1996). The coefficients in the x and z directions were always equal at the same depth in order to ensure that soil resistance was uniform around the pile.

Detailed Stress Analysis

Differential settlements are known to add stresses to statically indeterminate bridges after they are imposed. Accordingly, it is important to analyze the bridge using a refined stress-based finite element analysis to identify locations of high stress concentration. Abaqus was chosen since it is one of the top-rated multi-physics finite element analysis packages and the most widely used in research and practice worldwide. Therefore, it has been implemented to perform a refined and detailed finite element stress analysis. Three element types were used; Solid elements, shell elements, and beam elements. A 20-node quadratic brick, reduced integration (C3D20R) element was used for the solid meshes in the abutments, pier cross-beams, pier columns, and pile caps. An 8-node doubly curved thick shell elements, with

reduced integration scheme (S8R) were used for box girders. A 3-node quadratic beam in 3D space (B32) elements were used for the piles under the piers and abutments. A refined element size of 0.25 ft. was used for the regions where stress concentration occurs such as pier columns and abutments, while an element size of 0.5 ft. was used for box girders, and element size of 1.0 ft. was used for the beam elements in piles. In total, the model is made of 745 beam elements, 56,544 shell elements, 130,968 solid elements and 767,909 nodes. The model neglects the rebar present in the concrete.

In order to restrain the parts in the assembly, different types of restraining elements were used. Tie elements were used to restrain solid mesh parts to each other in the assembly. The shell to solid coupling was used to restrain contacts between shell and solid elements. And the meshes of same kind were merged in the box girders in order to reduce recurring nodes in the contact. Linear springs were modeled in the piles to connect the piles to the surrounding soil. The types of restrains are shown in Figure 9.

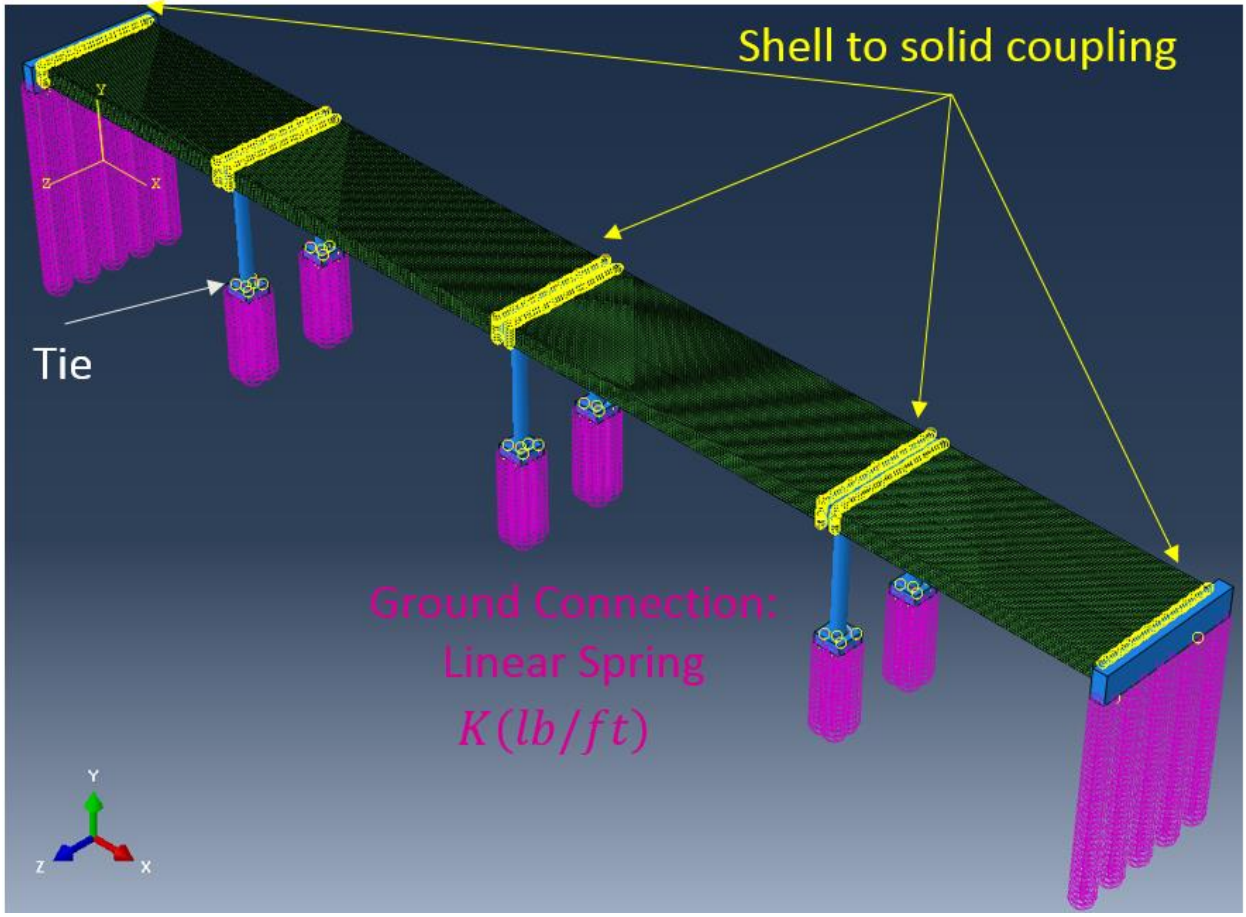

Figure 9: Types of Restraining Elements used in the Abaqus Model

Generalized Structural Analysis

The commercial finite element software, RISA3D, was used to model the bridge in this part. Three element types were used; linear solid elements, linear shell elements, and beam elements. An 8-node linear brick element was used for the solid meshes in the abutments, pier cross-beams, and pile caps. A 4-node linear plate element was used for box girders. A 2-node cubic beam element in 3D space was used for the piles under the piers and abutments as well as the piers themselves. The mesh used was made as fine as possible without exceeding the number of plate elements the program allows or without making the element aspect ratio closer to a solid element rather than a thin plate element. In total, the model is made of 516 beam elements, 33,600 plate elements, 6,784 solid elements and 43,044 nodes. Like the Abaqus model, the rebar is not included in the RISA model. This model is shown below in Figure 10.

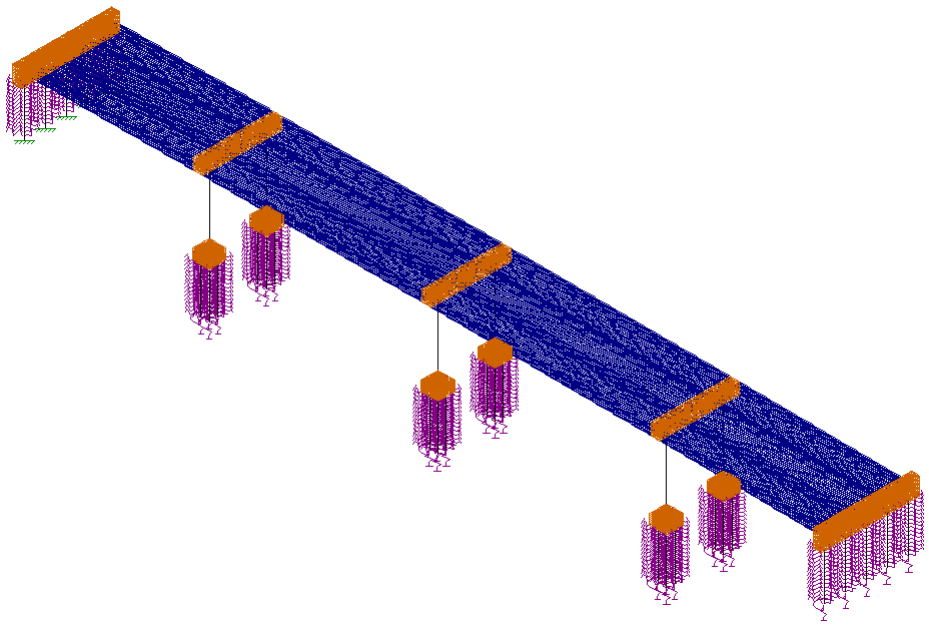

Figure 10: RISA 3D Model with Plates Modeling All Spans

The Abaqus model gives its results in terms of element stresses, which is valuable because the results show how the local stress changes throughout the element or throughout a full component. However, there is no direct way to know the resultant forces and moments acting on the component section to

establish an interaction diagram. RISA 3D presents the results as separate bending moment, axial and shear forces acting on the member or component, which allows the forces/moments to be mapped onto the limit state interaction diagrams with the rebar included. This feature is available for the beam and plate elements but not for the solid elements. After the different interaction curves are developed, the forces can be extracted and plotted to see if a component reaches a limit state.

Types of Analysis

Settlement Analysis

Each of the models was analyzed using the same process. The analysis was broken into two steps, first each pile in the model, with the exception of the piles under abutment 1, were placed on vertical springs and were allowed to naturally settle under self-weight until the settlement was as close to the settlement measured in April 2013 as possible. The piles under abutment 1 remained fixed at their base since abutment 1 has not effectively settled. This process was accomplished by adjusting the vertical spring coefficients in an iterative process until the settlements were as close to the final settlement without any of the points exceeding the settlement at that specific location. After the vertical coefficients were finalized, the model generated the forces and stresses within each element. In step 2 of the analysis, the model was fixed at all locations at the bridge's original elevations and displacements were imposed on the bottom of the piles to match the total settlement in the bridge on April 2017. By imposing the settlements at the bottom of the piles, the bridge would be pulled down, creating some tension in the piles and piers, until the total settlement was reached. The imposed displacements were added at pier 1 south, pier 2 south, pier 2 north, and pier 3 south, where the natural settlement from stage 1 did not match the total settlement of the bridge. After the displacements were imposed, the models generated the forces and stresses within each element. The forces and stresses from each step were then added together to determine the total forces and stresses that were acting on the bridge. These forces and stresses represent the current state of the bridge, based on the most recent survey data in April 2017.

Projected Settlement Schemes

Based on the settlement data available until April 2017, projected settlements until April 2022 under 6 different schemes were developed to study the possibility of failure in any of the bridge components. The analysis continued for each scheme until April 2022 or until failure is indicated in the specific component under investigation. Each scheme summed the year to year differential settlements from April 2014 to April 2017 at each abutment and pier location and then applied the projected settlement at the same location. The following criteria show how the projected settlements for the different schemes are established.

Scheme I:

The total incremental settlements of April 2014 to April 2017 are summed up and the average is determined by dividing by 4. This average is used as a constant settlement increment for each year starting April 2018 to April 2022.

$$Ave = \frac{Apr14 + Apr15 + Apr16 + Apr17}{4}$$

$$Apr18 = Ave, Apr19 = Ave, Apr20 = Ave, Apr21 = Ave, Apr22 = Ave$$

Scheme II:

The total incremental settlements of April 2014 to April 2017 are summed up. This sum is used as a constant settlement increment for each year starting April 2018 to April 2022 multiplied by a modifying fraction such that the total four-year increment is kept the same.

$$Sum = Apr14 + Apr15 + Apr16 + Apr17$$

$$Apr18 = Sum \times \frac{5}{16}, Apr19 = Sum \times \frac{3}{16}, Apr20 = Sum \times \frac{5}{16},$$

$$Apr21 = Sum \times \frac{3}{16}, Apr22 = Sum \times \frac{5}{16}$$

Scheme III:

The total incremental settlements of April 2014 to April 2017 are summed up and the average is determined by dividing by 4 and multiplying by 1.25. This augmented average is used as a constant settlement increment for each year starting April 2018 to April 2022.

$$Ave_m = \frac{Apr14 + Apr15 + Apr16 + Apr17}{4} \times 1.25$$

$$Apr18 = Ave_m, Apr19 = Ave_m, Apr20 = Ave_m, Apr21 = Ave_m, Apr22 = Ave_m$$

Scheme IV:

The total incremental settlements of April 2014 to April 2017 are summed up and multiplied by 1.25. This augmented sum is used as a constant settlement increment for each year starting April 2018 to April 2022 multiplied by a modifying fraction such that the total four-year increment is kept the same.

$$Sum_m = (Apr14 + Apr15 + Apr16 + Apr17) \times 1.25$$

$$Apr18 = Sum_m \times \frac{6}{16}, Apr19 = Sum_m \times \frac{2}{16}, Apr20 = Sum_m \times \frac{6}{16},$$

$$Apr21 = Sum_m \times \frac{2}{16}, Apr22 = Sum_m \times \frac{6}{16}$$

Scheme V:

The total incremental settlements of April 2014 to April 2017 are summed up and the average is determined by dividing by 4 and multiplying by 1.5. This augmented average is used as a constant settlement increment for each year starting April 2018 to April 2022.

$$Ave_n = \frac{Apr14 + Apr15 + Apr16 + Apr17}{4} \times 1.5$$

$$Apr18 = Ave_n, Apr19 = Ave_n, Apr20 = Ave_n, Apr21 = Ave_n, Apr22 = Ave_n$$

Scheme VI:

The total incremental settlements of April 2014 to April 2017 are summed up and multiplied by 1.5. This augmented sum is used as a constant settlement increment for each year starting April 2018 to April 2022 multiplied by a modifying fraction such that the total four-year increment is kept the same. The settlement layout for Scheme VI along the north and south sides of the bridge is shown in Figures 11 and 12.

$$Sum_n = (Apr14 + Apr15 + Apr16 + Apr17) \times 1.5$$

$$Apr18 = Sum_n \times \frac{5}{16}, Apr19 = Sum_n \times \frac{3}{16}, Apr20 = Sum_n \times \frac{5}{16},$$

$$Apr21 = Sum_n \times \frac{3}{16}, Apr22 = Sum_n \times \frac{5}{16}$$

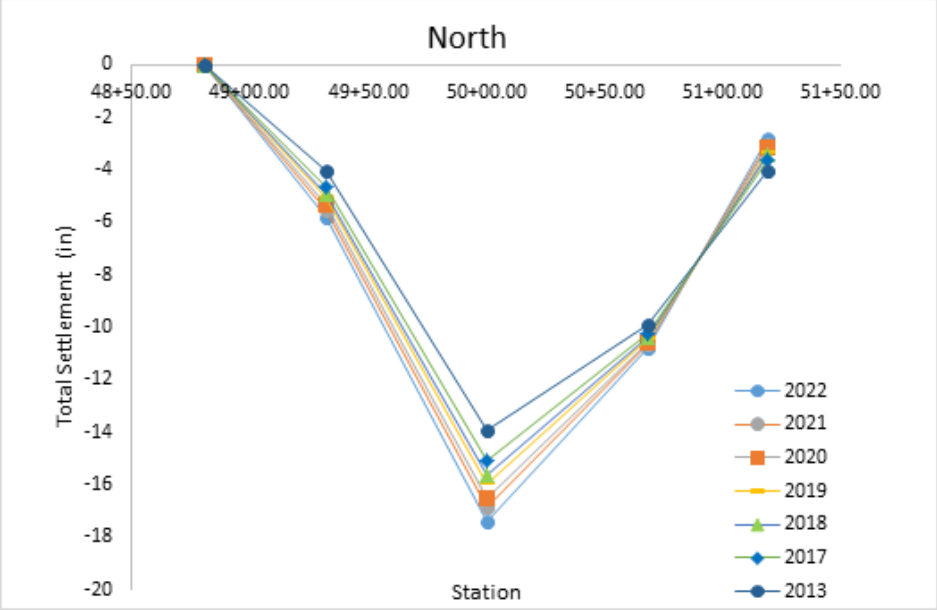

Figure 11: Scheme VI Actual and Projected Total Settlements from April 2013 – April 2022 at the North Piers and Abutments

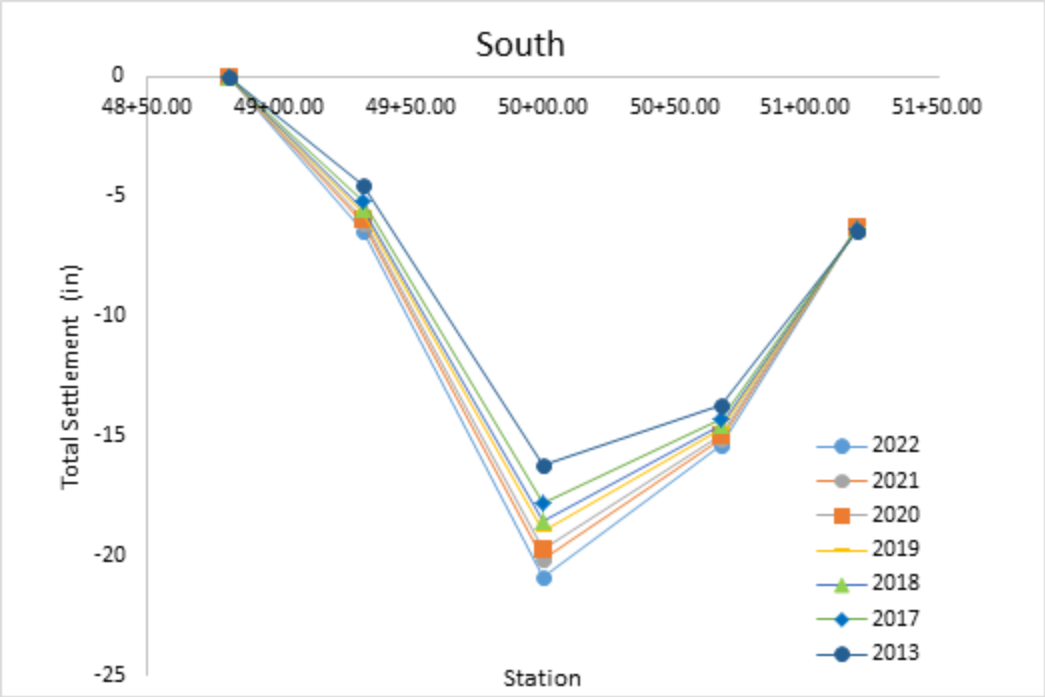

Figure 12: Scheme VI Actual and Projected Total Settlements from April 2013 – April 2022 at the South Piers and Abutments

Superimposed Live Load

In order to study the effect of live load superimposed with April 2017 settlements, a truck load (HS-20) of 72 kips total load was applied. The live load was applied at 8 different locations. Four of those locations were as the truck moves from west towards east of the bridge, and the other four locations were as the truck moves from east towards west bound. Figure 13 shows the magnitude and distance of applied live load from the edges at location 1 on span 1 while truck is moving from west towards east. This is deemed to be a critical analysis to perform to guarantee the safety of the bridge to crossing traffic.

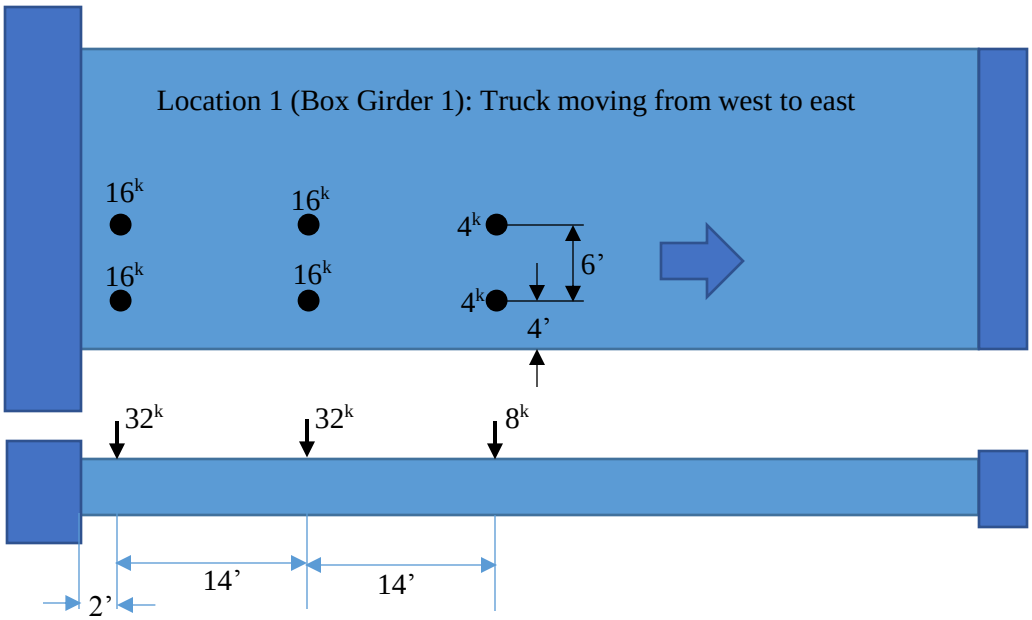

Figure 13: Positioning and Magnitudes of Superposed HS-20 Truck Loading

Results and Discussion

The results presented in the following section show the current state of the bridge in April of 2017. The projected settlement schemes and the truck loading yielded results similar to the ones shown below, but were not included in the report because of redundancy.

Stress Results of Various Components

The Abaqus results are mainly presented in terms of color-coded stress contour drawings for the various components of the bridge. It is important to indicate here that the threshold of concrete compressive strength (4000 psi) is set at the boundary of the red and orange color. This means that any red color showing up in the contour of colors indicates an exceedance of the concrete compressive strength. However, the red color in Figure 14 is irrelevant since it happens in the steel piles which have a yield strength of 36 ksi.

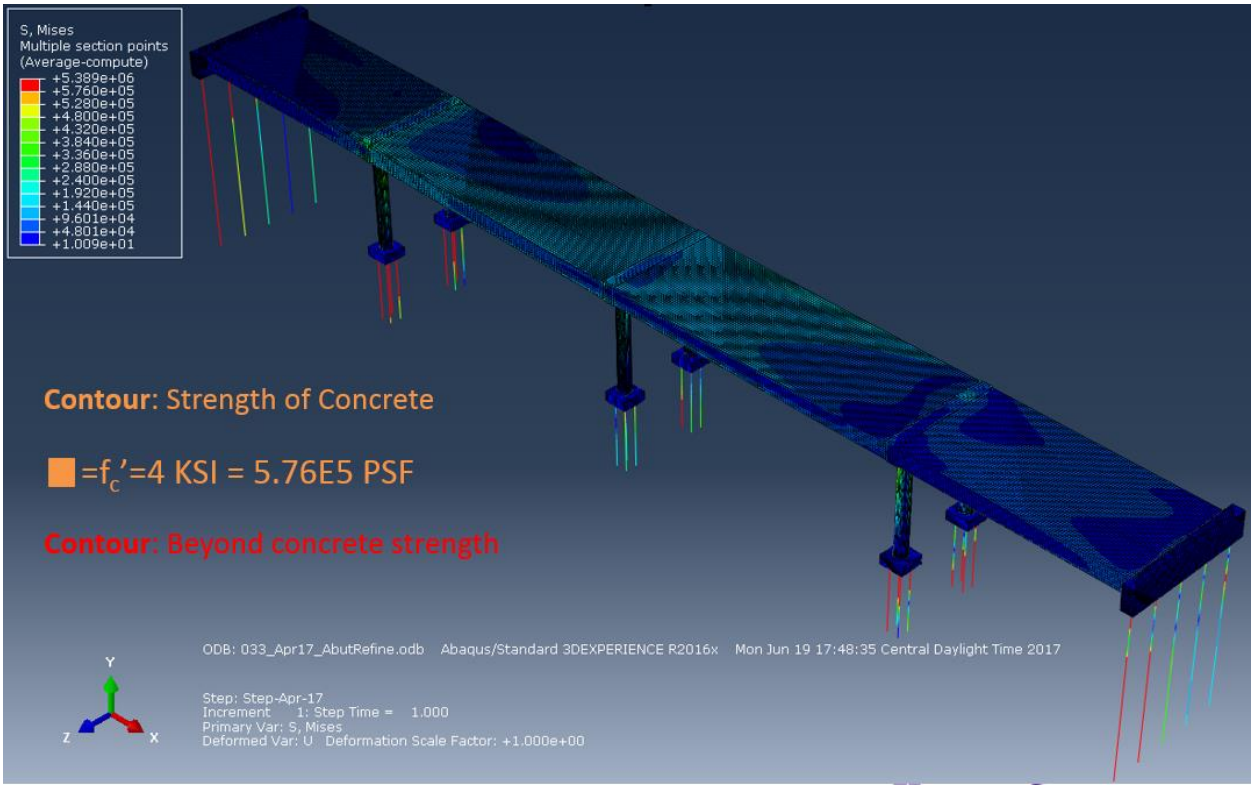

Figure 14: Von Mises Stress Distribution along the Bridge

Box Girder Results

The first two-step analysis performed is that of the settlements alone up to April 2017. The von Mises stress distribution on the box girders is shown in Figure 15. The stresses in the box girder are not critical where they are much lower than the 4 ksi strength of the concrete.

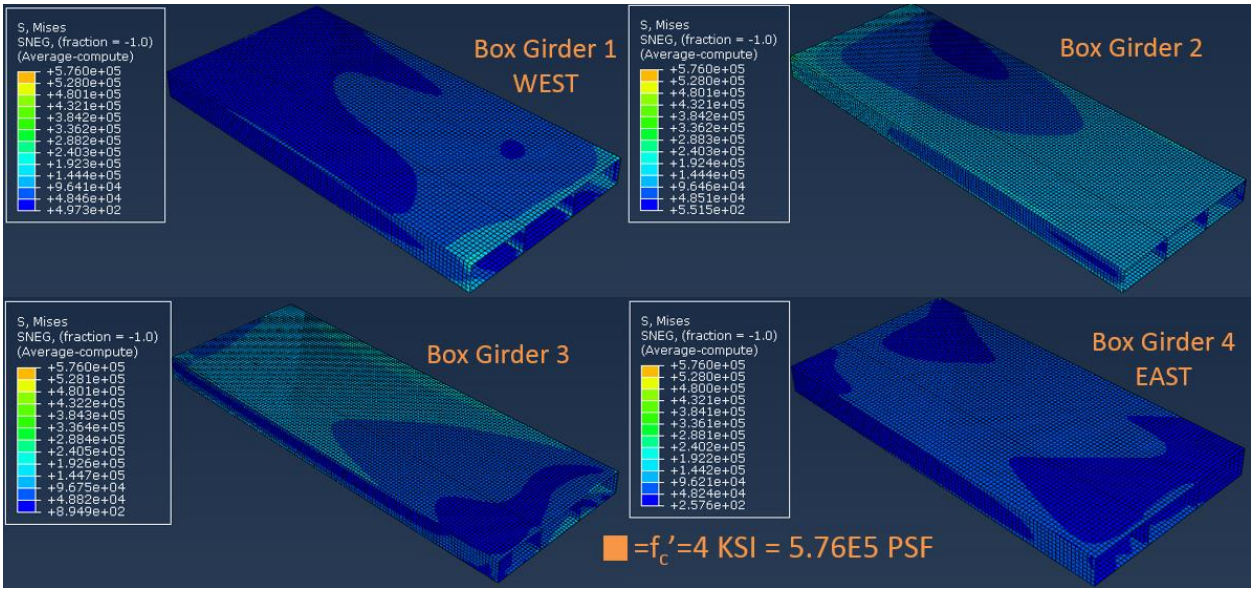

Figure 15: Von Mises Stress Distribution on the Box Girders

Pier Results

Figure 16 shows the von Mises stress contours of the cross-beams at piers. The maximum von Mises stress of cross-beams is much lower than strength of concrete. Therefore, cross-beams are not considered to be critical. The stresses of pier columns are shown in Figure 17 where a higher stress larger than the strength of concrete is observed at the top edge of the columns. These higher stresses are expected to be due to the stress concentration of the connection between and cross-beams and pier columns.

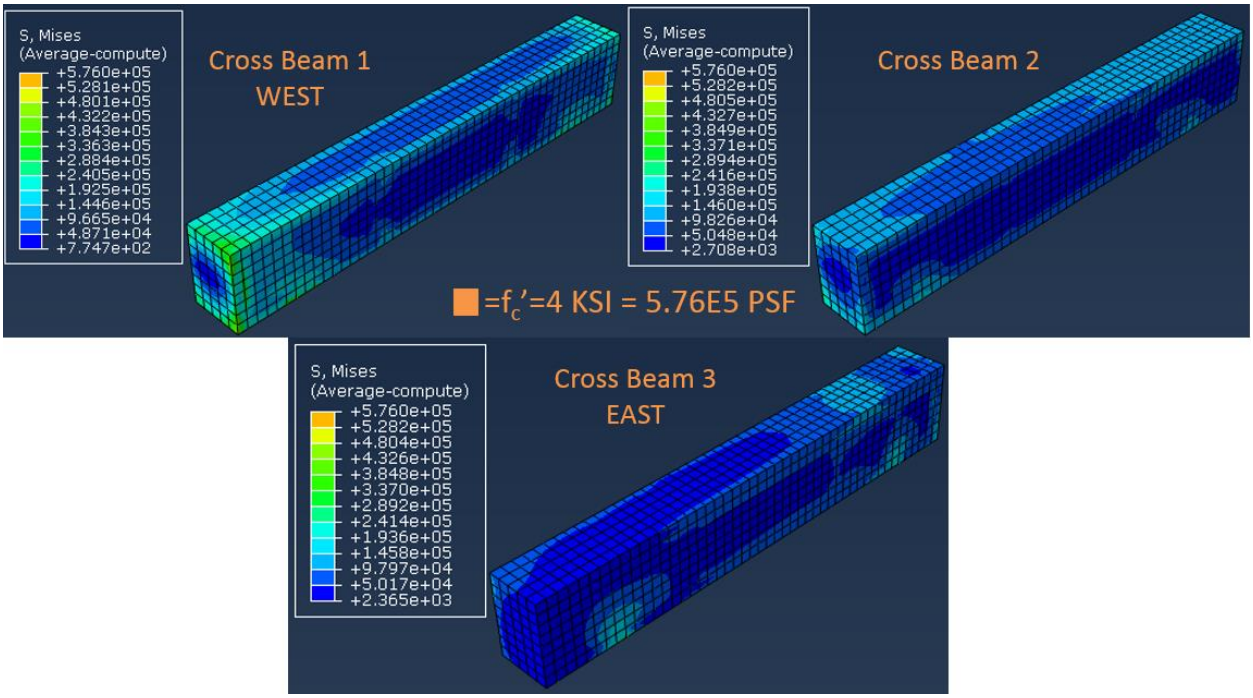

Figure 16: Von Mises Stress on the Cross-Beams at Piers

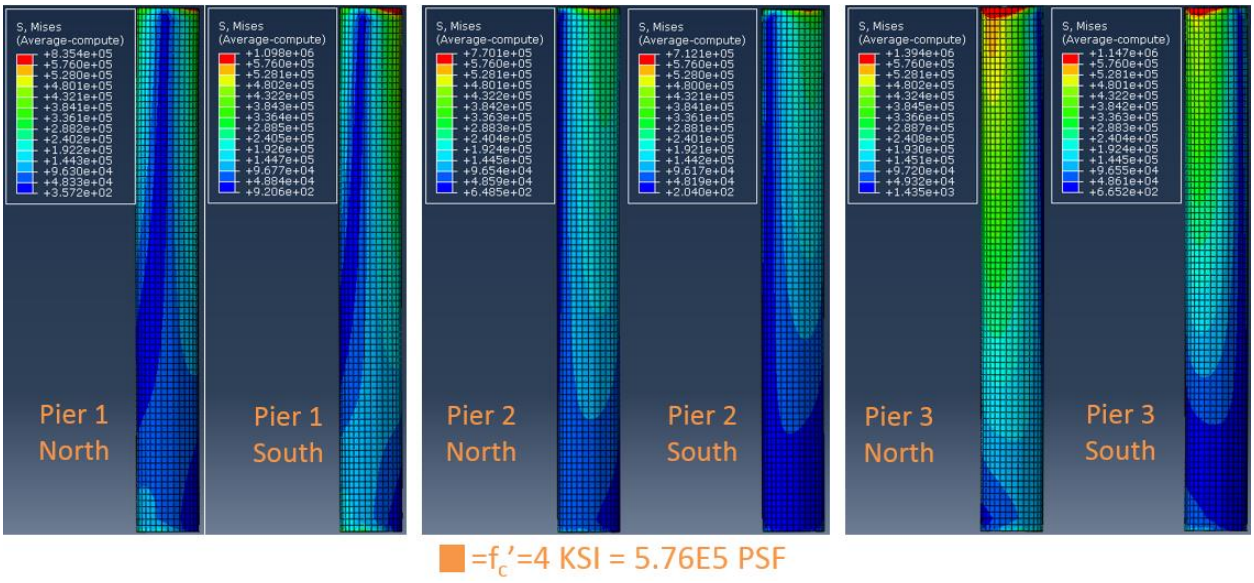

Figure 17: Von Mises Stress at Piers

The results from April 2017 show the same stress concentration beyond the concrete strength, which matches the current condition at the top of the pier, as seen in Figure 18. It is also important to mention

that the model doesn't consider the reinforcement embedded in the piers. The steel will take some of the load and lower the concrete's share of the stresses induced on the section.

Figure 18: Concrete Distress at Top of Pier

Pier and Abutment Pile Results

Figure 19 shows the von Mises stresses at the piles of abutments and piers. The maximum stress is observed at pile 1 of abutment 1, or the southernmost pile in the west abutment. The highest stress value is about two-thirds of the ultimate strength of steel, which doesn't fail. The nodal forces of the piles at the top, which may cause de-bonding shear stress at the embedded area between piles and pile caps, are also calculated. Based on Rabbat and Russell, an average bonding strength between steel and concrete is calculated to be 97 psi (57 psi bond strength and 40 psi shear strength), which is slightly on the conservative side. Whenever the shear stress increases beyond the limit of 97 psi at the embedded area, de-bonding is likely to occur. Based on the perimeters of the piles section, the embedment depth and bonding strength from Rabbat and Russell (1985), the maximum tensile nodal force should not be more than 82.5 kips at pier piles and 102.87 kips at abutment piles.

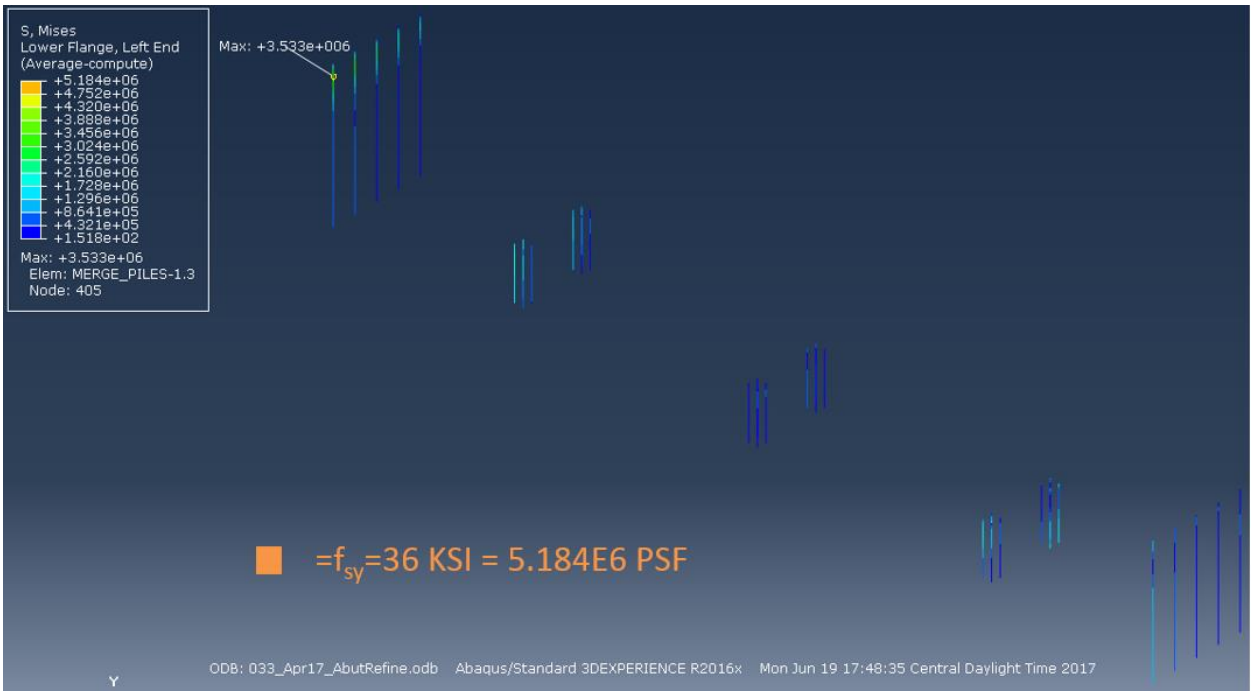

Figure 19: Von Mises Stress at Piles of Abutments and Piers

In case of tensile forces in the piles, it is important to evaluate the forces at the pile cap-pile intersection and compare it to the critical forces due to bond between the concrete and steel section. Figure 20 shows the location of piles at piers and abutments from top view. The numbering is shown as a reference to correctly read magnitude of nodal forces from related tables. Figures 21-25 show the deformation at the pile top-bottom of the pile cap junction to visually indicate a tension or compression force at each pile top by pulling out of or pushing into the pile cap. Tables 2 and 3 show the compressive and tensile nodal forces of piles at the piers and abutments, respectively. The positive value is tensile force while negative value is compressive force. The tables show that de-bonding will not occur when E=0.33E is used, but de-bonding likely occurs at pile 1 of pier 3 south column and if E=0.5E is used.

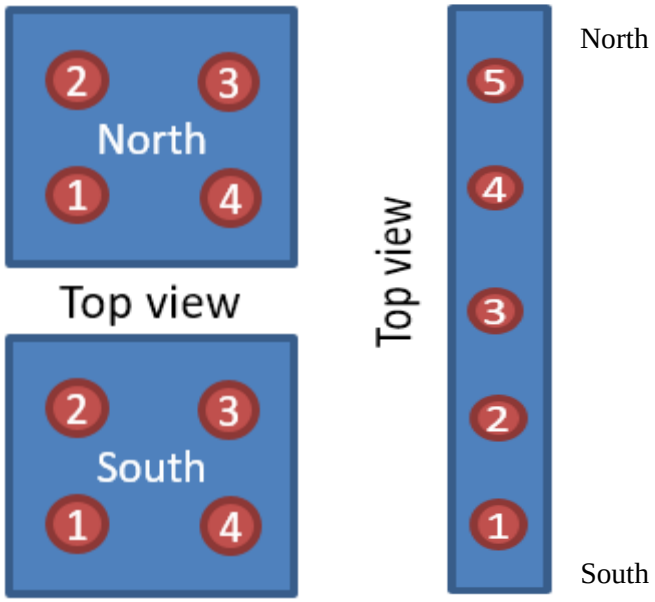

Figure 20: Location of Piles at Piers and Abutments: Pier (Left) and Abutment (Right)

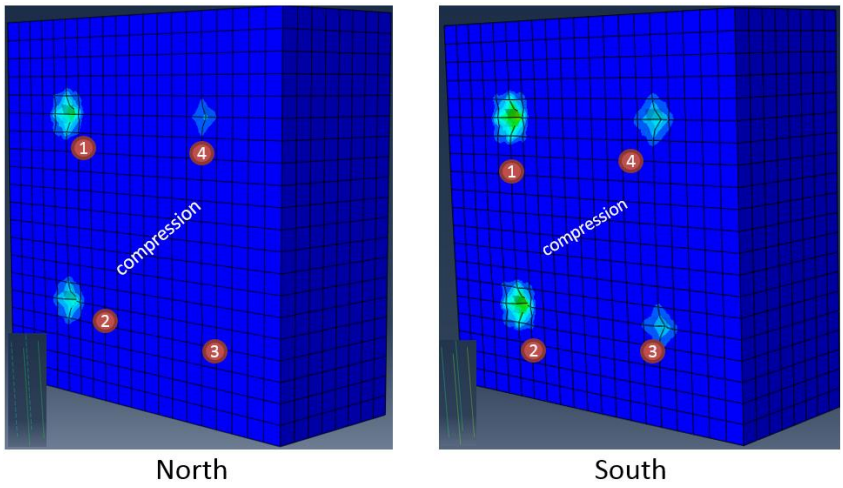

Figure 21: Pier 1 Piles-Pile Cap Junctions with Deformation

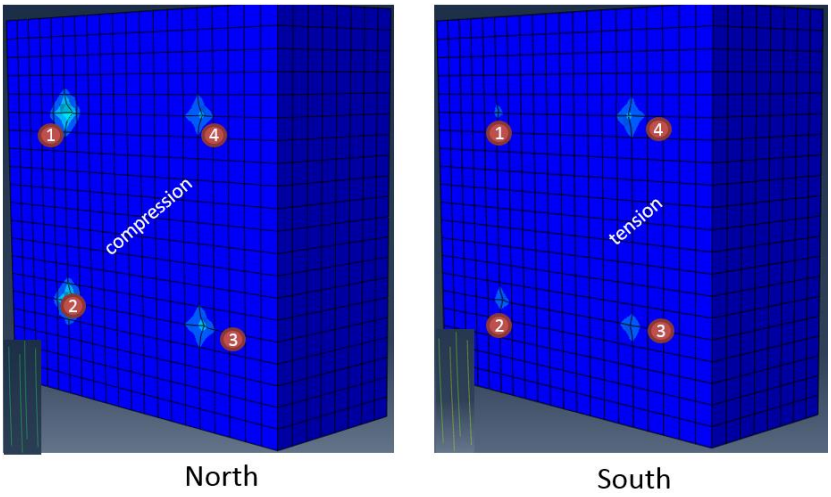

Figure 22: Pier 2 Piles-Pile Cap Junctions with Deformation

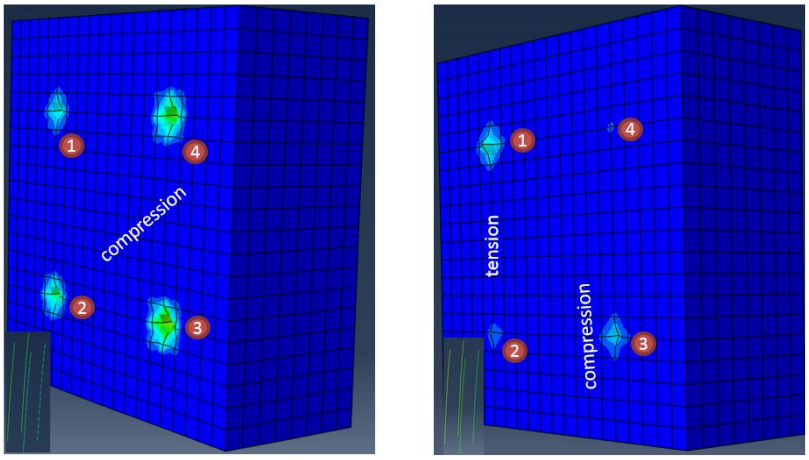

Figure 23: Pier 3 Piles-Pile Cap Junctions with Deformation

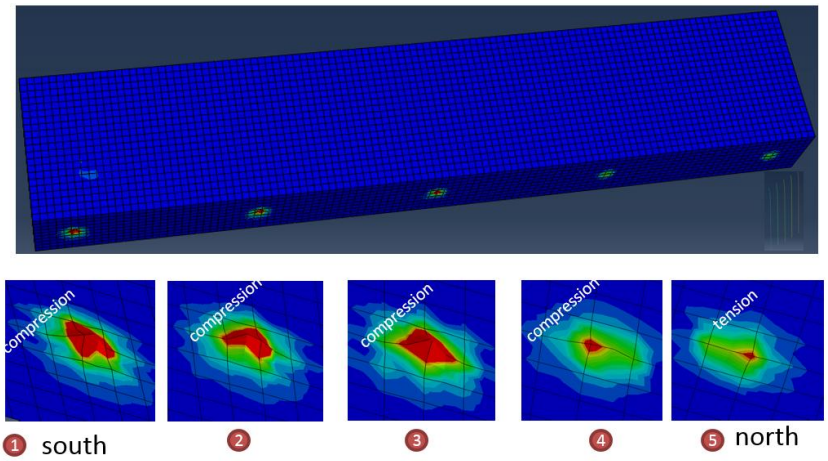

Figure 24: Abutment 1 Piles-Abutment Junctions with Deformation

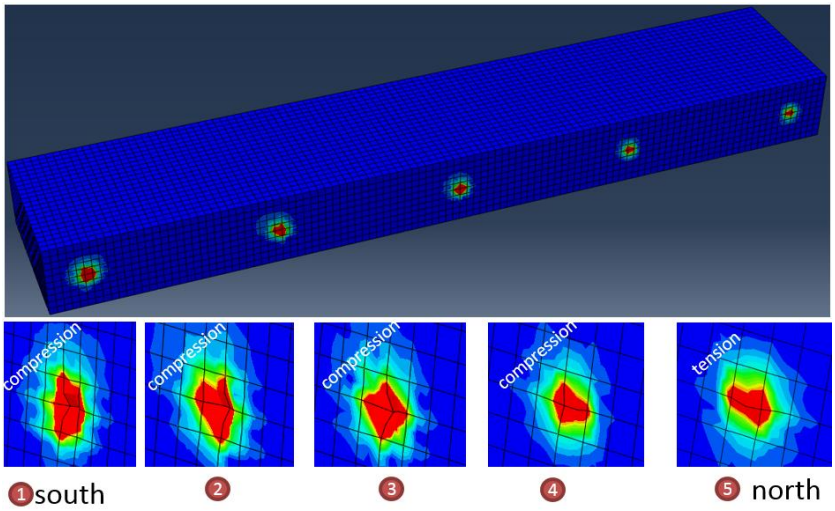

Figure 25: Abutment 2 Piles-Abutment Junctions with Deformation

Table 2: Pile Nodal Forces at the Pile Cap of the Piers

Pier 1 Pile (Nodal force at piles top) Pullout starts at 82.5 kips				
		North		
	Pile 1	**Pile 2**	**Pile 3**	**Pile 4**
Forces	NFORCSO1	NFORCSO1	NFORCSO1	NFORCSO1
E=0.5E	-123.123	-85.566	11.728	-25.819
E=0.33E	-104.16	-77.925	-2.702	-28.927
		South		
	Pile 1	**Pile 2**	**Pile 3**	**Pile 4**
Forces	NFORCSO1	NFORCSO1	NFORCSO1	NFORCSO1
E=0.5E	-198.11	-173.679	-51.652	-76.068
E=0.33E	-152.871	-138.641	-44.715	-58.93
Pier 2 Pile cap (Nodal force at piles top)				
		North		
	Pile 1	**Pile 2**	**Pile 3**	**Pile 4**
Forces	NFORCSO1	NFORCSO1	NFORCSO1	NFORCSO1
E=0.5E	-67.912	-68.189	-26.888	-26.609
E=0.33E	-64.208	-67.921	-35.222	-31.509
		South		
	Pile 1	**Pile 2**	**Pile 3**	**Pile 4**
Forces	NFORCSO1	NFORCSO1	NFORCSO1	NFORCSO1
E=0.5E	1.065	-0.189	60.832	62.095
E=0.33E	-16.218	-23.007	24.317	31.112
Pier 3 Pile cap (Nodal force at piles top)				
		North		
	Pile 1	**Pile 2**	**Pile 3**	**Pile 4**
Forces	NFORCSO1	NFORCSO1	NFORCSO1	NFORCSO1
E=0.5E	-92.723	-133.064	-220.856	-180.503
E=0.33E	-72.406	-108.639	-173.3	-137.058
		South		
	Pile 1	**Pile 2**	**Pile 3**	**Pile 4**
Forces	NFORCSO1	NFORCSO1	NFORCSO1	NFORCSO1
E=0.5E	108.583	58.319	-32.217	18.048
E=0.33E	68.941	23.189	-44.378	1.376

Table 3: Pile Nodal Forces at the Abutments

Abutment 1 (Nodal force at piles top) Pullout starts at 102.87 kips					
	Pile 1	**Pile 2**	**Pile 3**	**Pile 4**	**Pile 5**
Forces	NFORCSO1	NFORCSO1	NFORCSO1	NFORCSO1	NFORCSO1
E=0.5E	-70.156	-45.612	-17.658	10.612	44.888
E=0.33E	-58.342	-40.915	-19.686	-2.035	21.862
Abutment 2 (Nodal force at piles top)					
	Pile 1	**Pile 2**	**Pile 3**	**Pile 4**	**Pile 5**
Forces	NFORCSO1	NFORCSO1	NFORCSO1	NFORCSO1	NFORCSO1
E=0.5E	-126.789	-82.376	-32.273	-3.947	33.641
E=0.33E	-99.502	-66.291	-27.297	-10.792	14.905

Force Moment Interaction Diagrams

Box Girder Results

The box girder section is divided into individual rectangular components to facilitate its interaction diagram analysis. Three main components are identified namely, a top horizontal panel in between two webs, a bottom horizontal panel in between two webs and a single vertical web panel. The top and bottom slab has been divided into three sections: the north, middle, and south sections. There are four separate webs in the box girder. Below, the individual analysis of each component is presented at span 2 of the bridge (critical span) shown at five sections of the box girder: next to pier 1, the quarter point, mid-span, the three quarters point, and next to pier 2. The points on the interaction diagrams represent the components at each of these sections. The interaction diagrams for each of these components were developed that included the concrete as well as the steel reinforcement.

Top Flange of the Box Girder

Each of the top slab sections has a width of 98 inches, a thickness of 7 inches and a clear cover to reinforcement of 2 inches. The amount of reinforcement varies along the span. However, the maximum reinforcement of 20 # 9 bars and 14 # 5 bars is used to plot the interaction diagram since exceeding the limits of this diagram refers to a possible failure regardless. Figure 26 shows five points exceeding the diagram limits on the tension side suggesting the critical state of the top slab under April 2017 settlements.

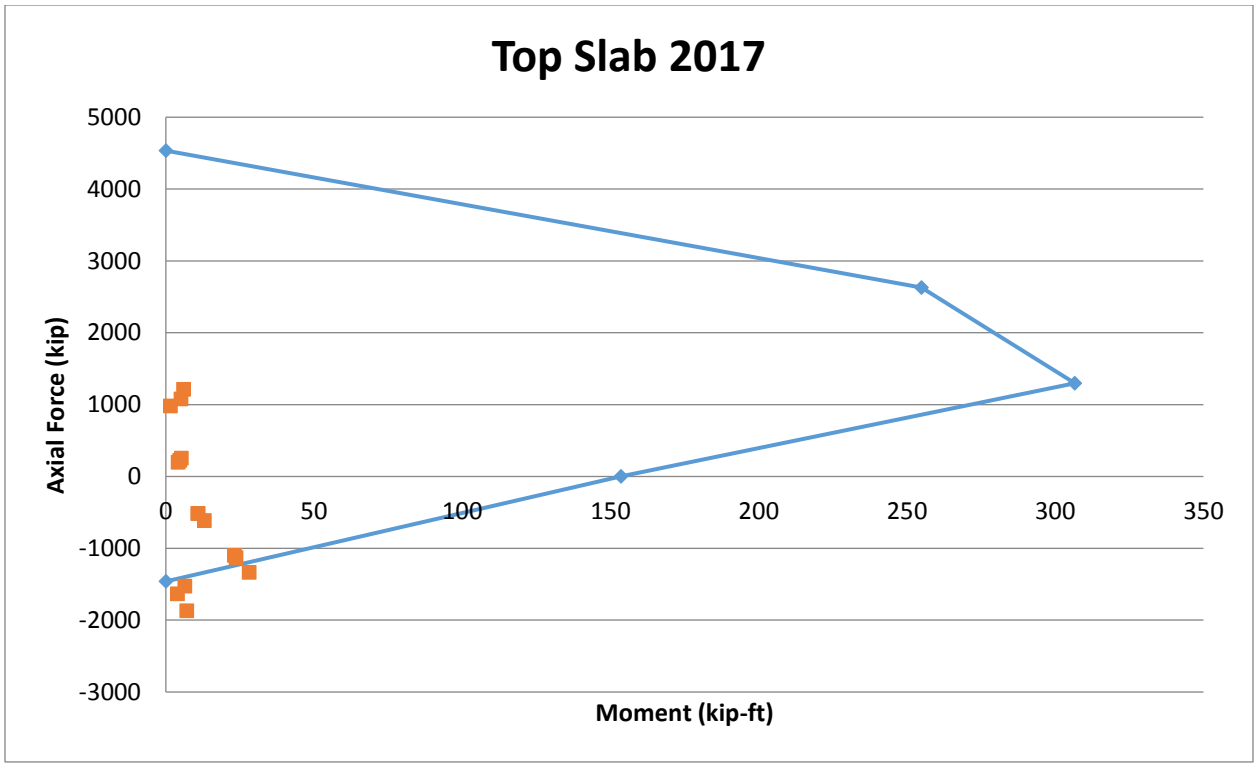

Figure 26: Interaction Diagram for the Top Slab at Span 2

Bottom Flange of the Box Girder

Each of the bottom slab sections has a width of 98 inches, a thickness of 6 inches and a clear cover to reinforcement of 1 inch. The amount of reinforcement varies along the span. However, the maximum reinforcement of 16 # 8 bars is used to plot the interaction diagram since exceeding the limits of this diagram refers to a possible failure regardless. Figure 27 shows three points exceeding the diagram limits on the tension side suggesting the critical state of the bottom slab under April 2017 settlements.

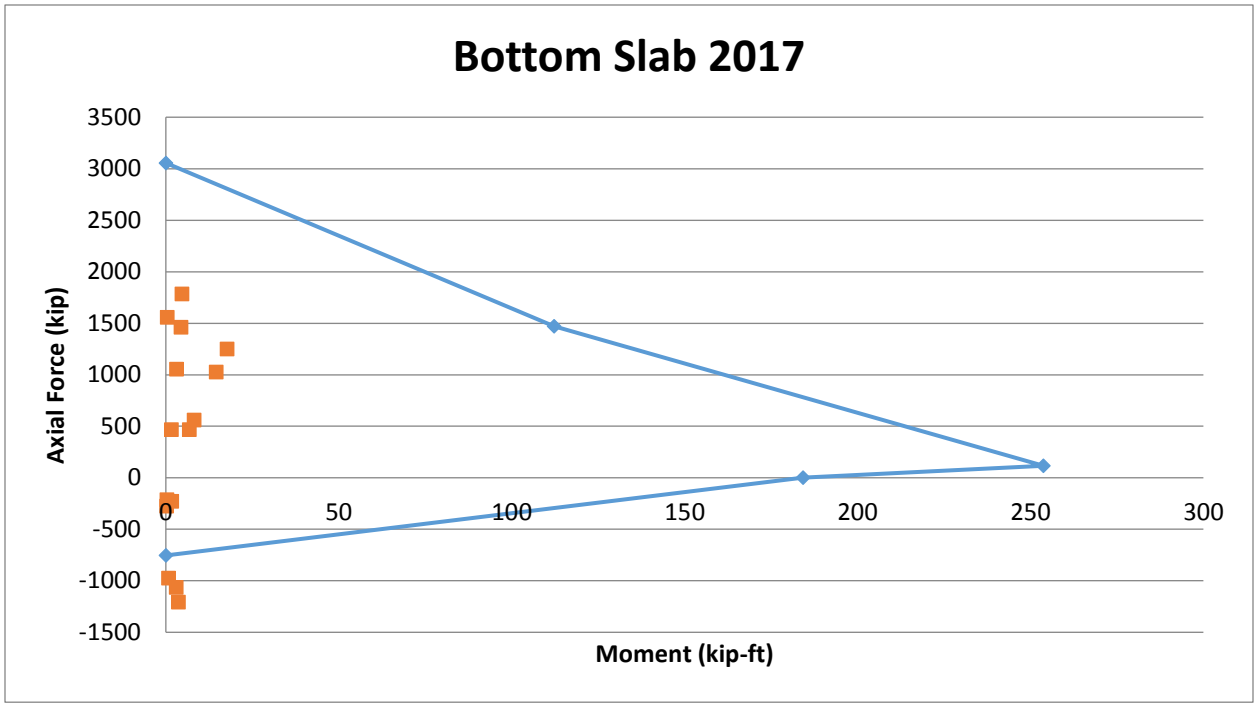

Figure 27: Interaction Diagram for the Bottom Slab at Span 2

Web of Box Girder

The web vertical slab has a height of 42 inches, a thickness of 8.5 inches and a clear cover to reinforcement of 1 inch. The amount of reinforcement is constant along the span with 2 #8 bars and 4 #5 bars. However, the longitudinal reinforcement of 6 # 6 bars is used to plot the interaction diagram to simplify the analysis, while maintaining the same steel area. Figure 28 shows several points exceeding the diagram limits along the moment axis suggesting the critical state of the web slab under April 2017 settlements.

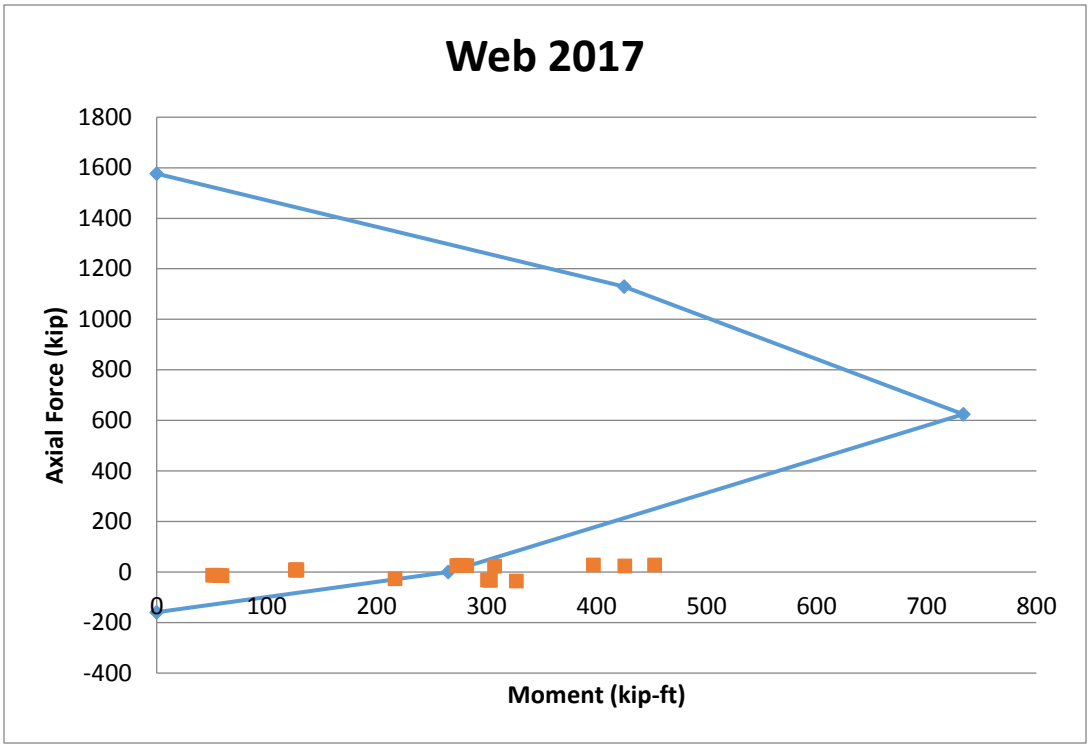

Figure 28: Interaction Diagram for the Web Slab at Span 2

Pier Results

The pier column section has a diameter of 30 inches and a clear cover to reinforcement of 2 inches. The longitudinal reinforcement of 9 # 8 bars is used to plot the interaction diagram. Each one of the six piers represents a point on the interaction diagram. Figure 29 show a single point slightly exceeding the diagram limits along the tension force axis suggesting it is close to the critical state of at least one of the pier columns under April 2017 settlements.

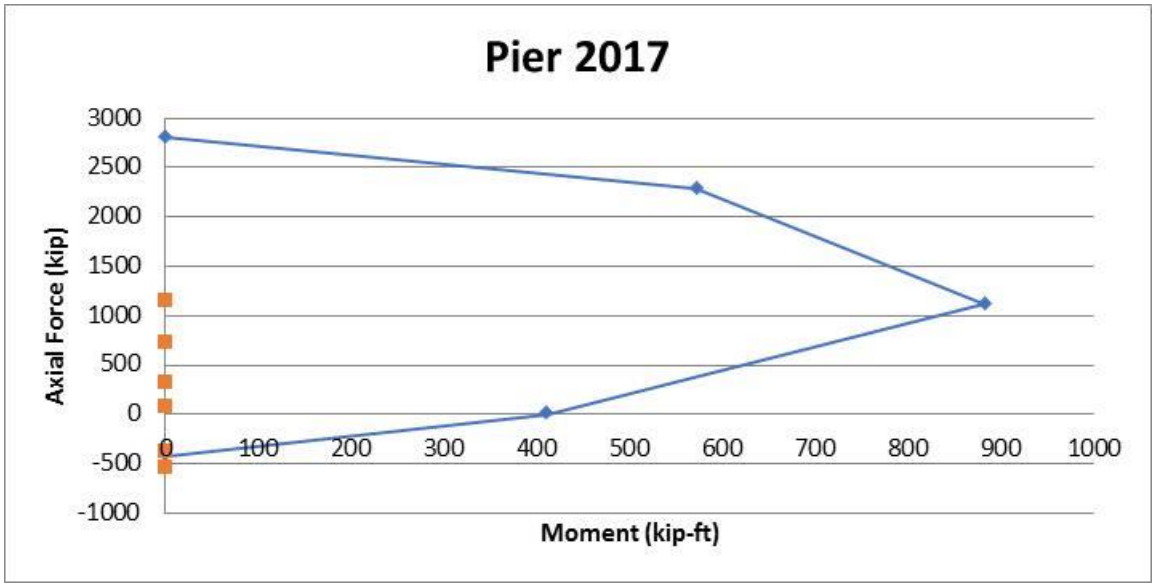

Figure 29: Interaction Diagram for the Piers

Pile Results

The interaction diagram for the pier piles is computed using Excel assuming a uniaxial moment-axial compression force with yield strength of 36 ksi. Figure 30 presents the points mapped on the interaction diagram. It is evident from Figure 30 that the pier piles are all safe since they are well within the interaction diagram.

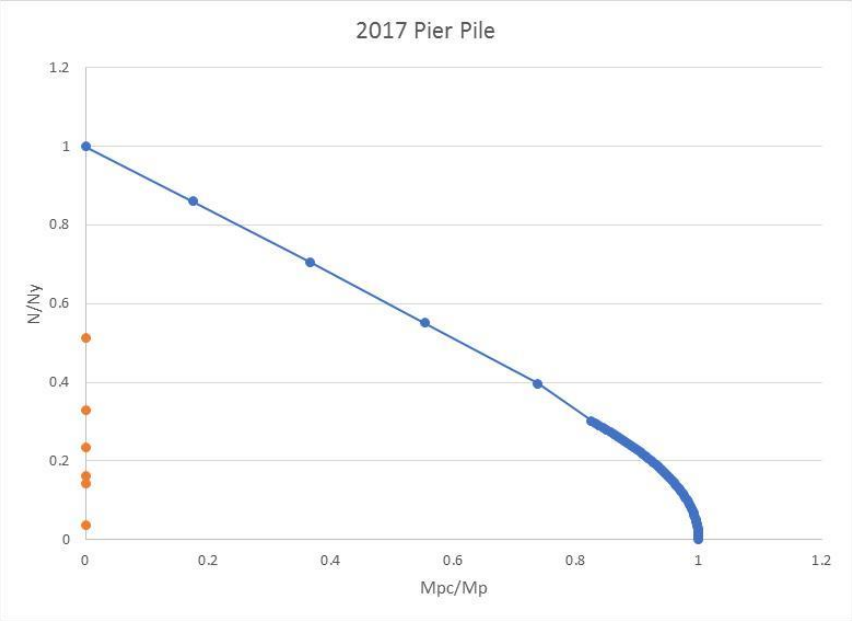

Figure 30: Interaction Diagram for the Pier Piles

The interaction diagram for the abutment piles is computed using Excel assuming a uniaxial moment-axial compression force with yield strength of 36 ksi. Figure 31 presents the points mapped on the interaction diagram. It is evident from Figure 31 that the abutment piles are generally safe except for one point slightly outside the interaction diagram indicating proximity to being critical.

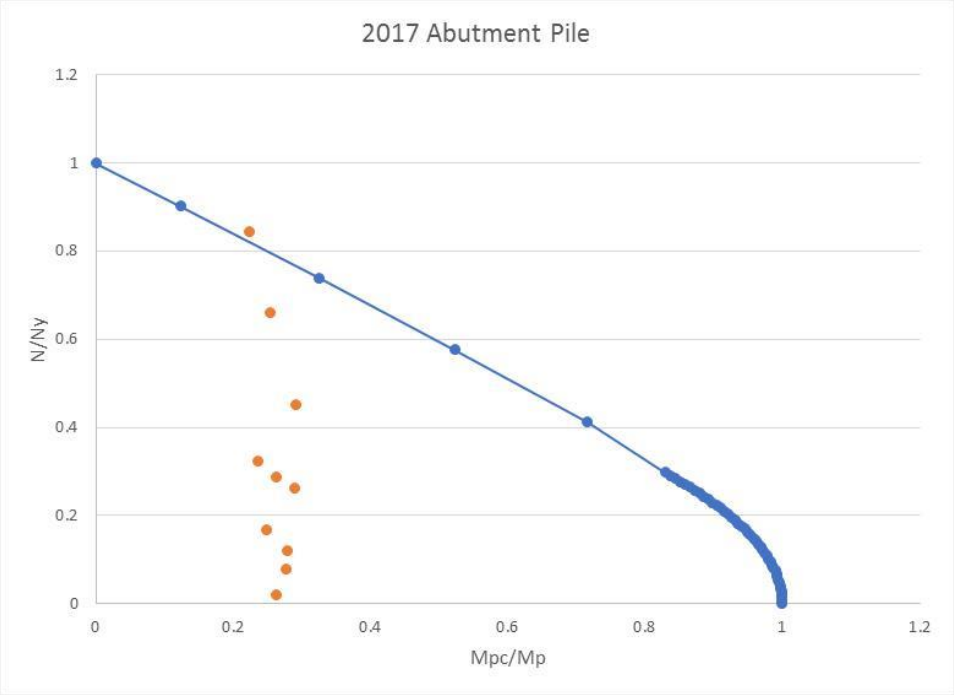

Figure 31: Interaction Diagram for the Abutment Piles

Box Girder Interaction Diagram

The plate results from the RISA model were used to analyze the bridge as one composite I-girder section, instead of treating each element of the box girder separately. All four of the webs from the box girder were combined to be one web with a thickness of 34 inches and height of 35 inches. The top and bottom slabs were both taken to have a width of 294 inches, with thicknesses of 7 inches and 6 inches, respectively. The rebar in the bridge was kept at the same depths as specified in the bridge plans. Figure 32 shows the adjustment made to the box girder.

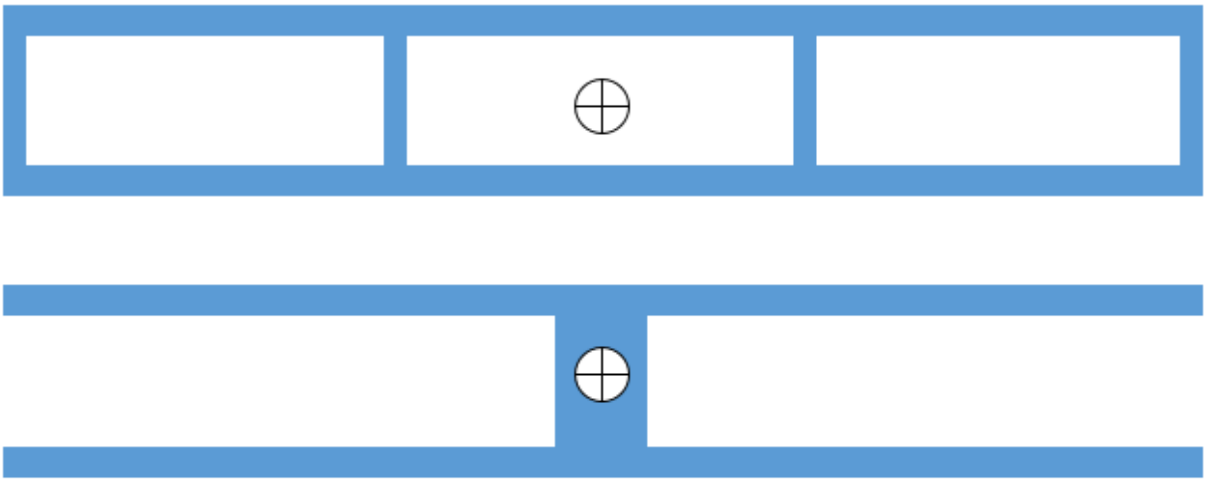

Figure 32: I Girder Transformation

A resultant axial force and bending moment was determined for the I-girder at five sections for each span, for a total of 20 points. These five sections in each span were located at the same spots, next to each pier, quarter point, mid-span, and three quarter point, as in the original RISA analysis. The resultant axial force was determined by the summation of the axial forces that were acting in each plate within the cross section of the I-girder. The axial forces occur at three different heights in the box girder according to the RISA model, the center of the top and bottom slabs, as well as the midpoint of the web. The axial force should act at the center of the I-girder, so the summation of the axial force was applied at the centroid, with moment applied to the I-girder to account for the eccentricities of the axial forces. The moments from the axial eccentricities were then summed with the moments occurring in each of the elements. The rebar within the I-girder changed at each location along the span and was adjusted accordingly to determine the capacity of each section. Figure 33 shows the interaction diagram for the midspan of Span 2. The two data points represent the bridge's condition in April 2017 and April 2022 under the worst case of the projected settlements, Scheme VI.

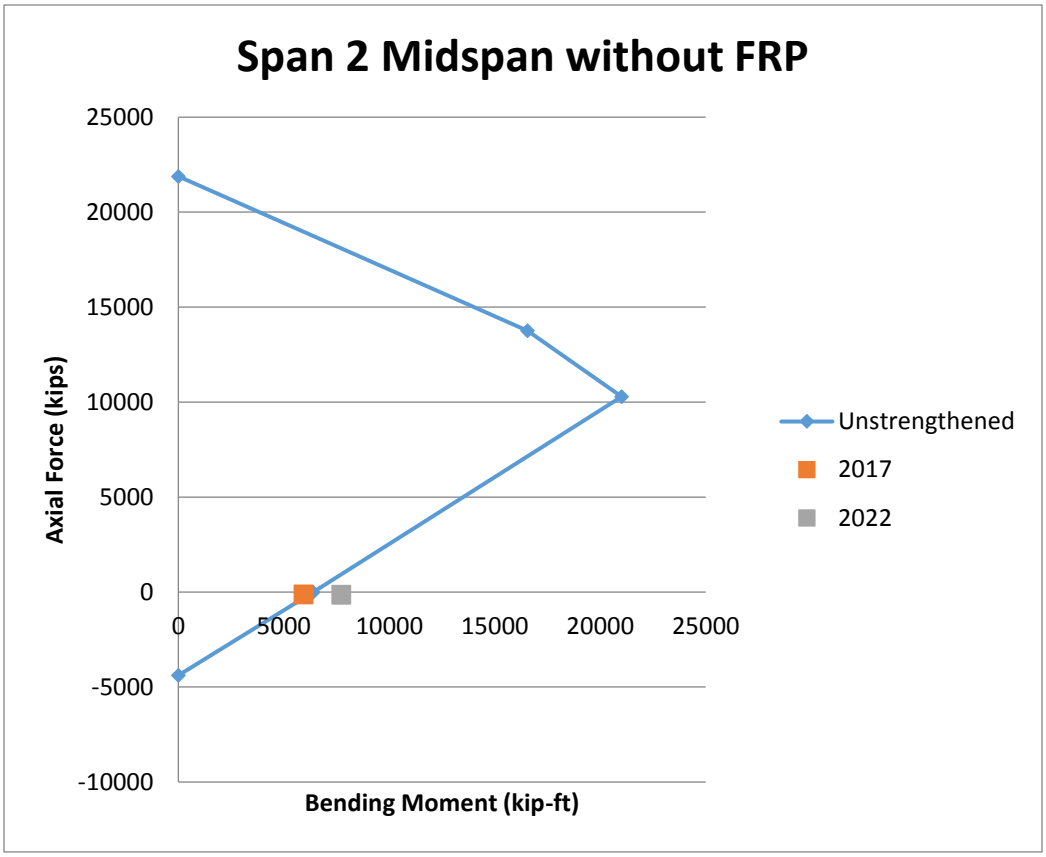

Figure 33: Interaction Diagram for Box Girder in the Midspan of Span 2

Fiber Reinforced Polymer Strengthening

At each location where the capacity of the I Girder was exceeded, near surface mounted Fiber Reinforced Polymer (FRP) rebar was added to the I-girder to increase the section's bending moment capacity to exceed the forces demanded by Scheme VI in 2022. The FRP rebar would be attached to the existing bridge by cutting a groove in the top or bottom of the box girder and placing the piece of rebar inside of the groove with epoxy. Two different types of FRP were used to strengthen the section, carbon fiber (CFRP) and glass fiber (GFRP). The carbon fiber bars used are #8 bars with a modulus of 18000ksi and ultimate elongation strain of 0.81%. The glass fiber bars used are #10 bars with a modulus of 6700ksi and ultimate elongation strain of 1.19%. Figure 34, shows the interaction diagram for same section of the box girder, the midspan of Span 2, which was shown in Figure 33, but with GFRP bars. The strengthening plan for each of the sections, puts enough FRP bars into the section so that it can withstand the projected settlement forces from Scheme VI in 2022.

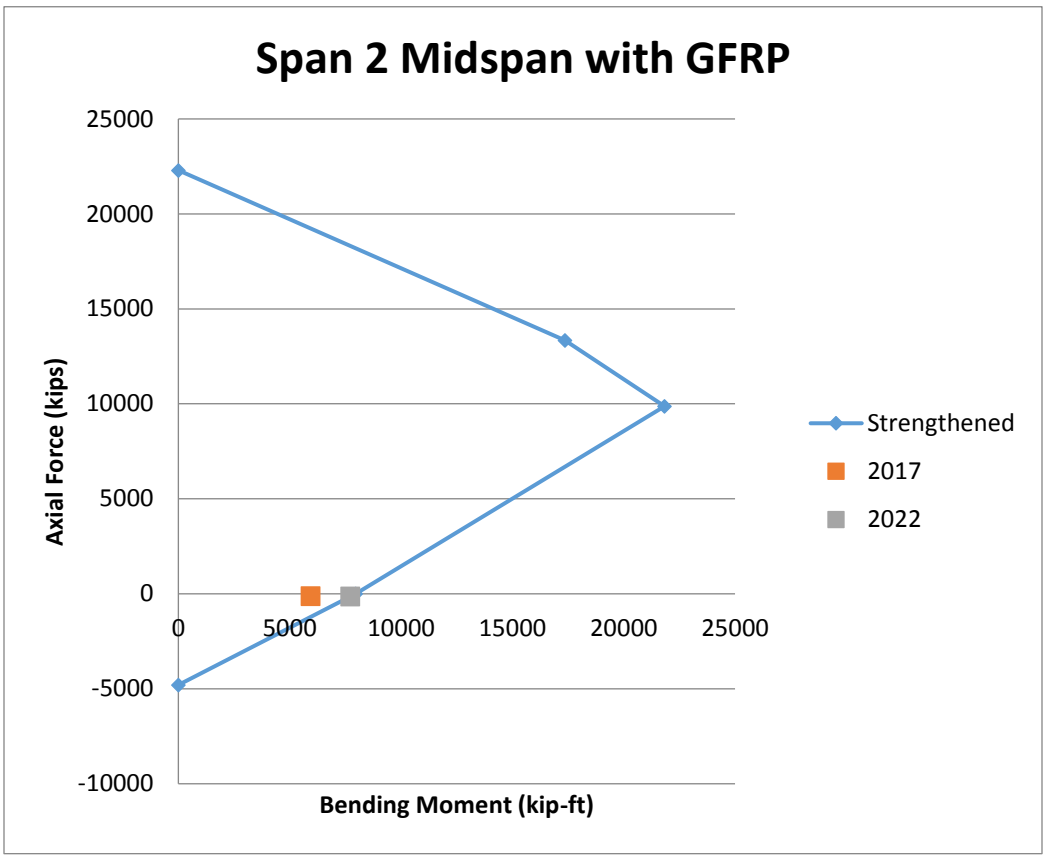

Figure 34: Interaction Diagram for Box Girder in the Midspan of Span 2 Strengthened with GFRP

Table 4 shows the total amount of each type of FRP bar that will be required to strengthen each of five sections for each span for flexure.

Table 4: Number of FRP Bars Required for Flexural Strengthening

		#10 GFRP	#8 CFRP
Span 1	Abutment 1	0	0
	1/4 Point	0	0
	Midspan	0	0
	3/4 Point	0	0
	Pier 1	36	31
Span 2	Pier 1	36	31
	1/4 Point	0	0
	Midspan	6	5
	3/4 Point	37	32
	Pier 2	26	22
Span 3	Pier 2	26	22
	1/4 Point	51	43
	Midspan	31	26
	3/4 Point	5	4
	Pier 3	0	0
Span 4	Pier 3	0	0
	1/4 Point	0	0
	Midspan	0	0
	3/4 Point	0	0
	Abutment 2	0	0

Shear and Torsion Analysis

The plate forces from the RISA 3D model were analyzed to see how the shear and torsional forces were combining to effect the box girder. This analysis was performed on the same five sections of the box girder for each span. Each section had to be analyzed separately based on the amount of shear reinforcement in the webs of the box girder, the amount of tensile reinforcement, and whether the section of the box girder was experiencing positive or negative flexure. The type of flexure experienced in each section determined whether the top or bottom slab of the box girder was in tension. This had to be found in order to accurately find the amount of tensile reinforcement present to resist yielding due to torsion. Figure 35 shows the shear flow that is found in the cross section that is on span 1 next to abutment 1 due to Scheme 6 projected settlement in 2022.

Figure 35: Shear Flow at Abutment 1

These values result in a net shear force of 102.64kips and a torsional moment of 3926.29 kip-ft. There is a positive bending moment of 682.7 kip-ft acting on the section as well. These values were compared to the capacity of the box girder as allowed by the American Association of State Highway and Transportation Officials (AASHTO). AASHTO limits the capacity of the section based on the spacing of the shear stirrups in the web, the yield strength of the tensile steel and the stress experienced in the concrete. In order to determine which of these factors were controlling for the section, interaction curves for the applied shear and torsion were developed using the equations developed from Halim et al. 2012 and the AASHTO code for shear and torsion design.

$$\frac{A_t f_{yt}}{s} = \frac{T_n}{2A_0 \cot\theta} + \frac{V_n - V_c}{2d_v \cot\theta} \qquad \text{Equation 5}$$

$$.25 f_c' \geq \frac{\left|V_u + \frac{T_u d_s}{2A_o}\right|}{\phi b_v d_v} \qquad \text{Equation 6}$$

$$A_s f_y \geq \frac{|M_u|}{\phi d_v} + \cot\theta \sqrt{\left(\frac{0.5V_u}{\phi} + 0.5V_c\right)^2 + \left(\frac{0.45P_h T_u}{2A_o \phi}\right)^2} \qquad \text{Equation 7}$$

The interaction curve for span 1, abutment 1 is shown in Figure 36.

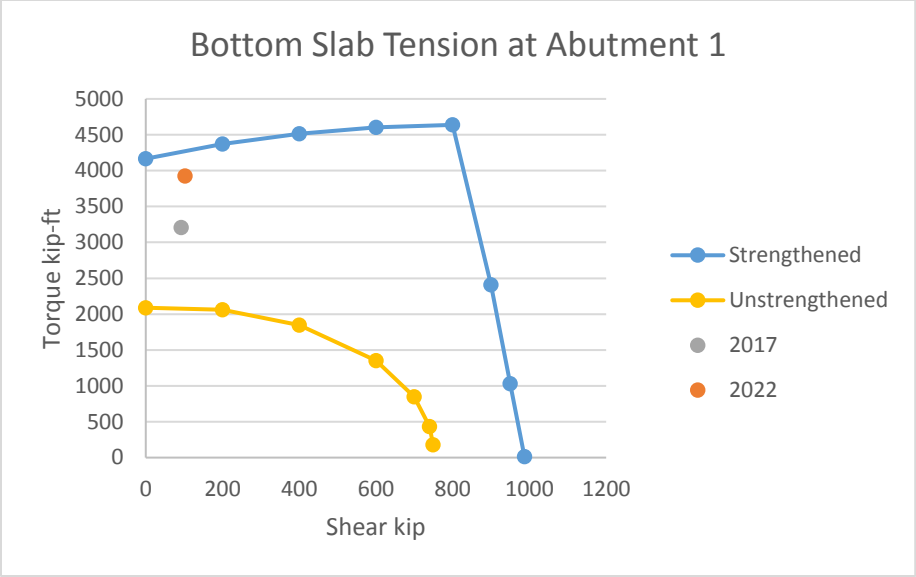

Figure 36: Shear and Torsion Interaction Curve at Abutment 1

The relatively flat part of the curve, until close to 1000 kips, is controlled by the yielding of the tensile reinforcement in the bottom slab, Equation 7. After this, the steep decline of the curve in controlled by the spacing of the shear stirrups, Equation 5. The concrete stress limited by Equation 6, did not control in this section, or any of the other sections that were analyzed. Since both the shear and torsion values from 2017 and 2022 exceed the capacity of the bridge in its current condition, a strengthening plan was developed so that all sections would have a capacity that exceeded the expected values from projected settlement scheme 6 in 2022. The strengthening plan involves near surface mounted CFRP and GFRP bars to be installed on the bridge similar to the flexural strengthening plan. This section failed where the tensile steel controlled, so near surface mounted FRP bars were added to the bottom section in order to increase the section's capacity. Table 5 shows the total number of FRP bars that will be added to the bridge at each section and the reason for their installation.

Table 5: Complete Strengthening Plan

		#10 GFRP	#8 CFRP	Reason
Span 1	Abutment 1	6	6	Torsion
	1/4 Point	0	0	
	Midspan	6	5	Torsion
	3/4 Point	21	18	Torsion
	Pier 1	60	52	Torsion and Flexure
Span 2	Pier 1	60	52	Torsion and Flexure
	1/4 Point	0	0	
	Midspan	16	14	Torsion and Flexure
	3/4 Point	51	44	Torsion and Flexure
	Pier 2	57	49	Torsion and Flexure
Span 3	Pier 2	57	49	Torsion and Flexure
	1/4 Point	64	55	Torsion and Flexure
	Midspan	44	38	Torsion and Flexure
	3/4 Point	14	12	Torsion and Flexure
	Pier 3	3	3	Torsion
Span 4	Pier 3	3	3	Torsion
	1/4 Point	0	0	
	Midspan	0	0	
	3/4 Point	0	0	
	Abutment 2	0	0	

Figures 37 and 38 show a complete plan for the GFRP and CFRP layouts.

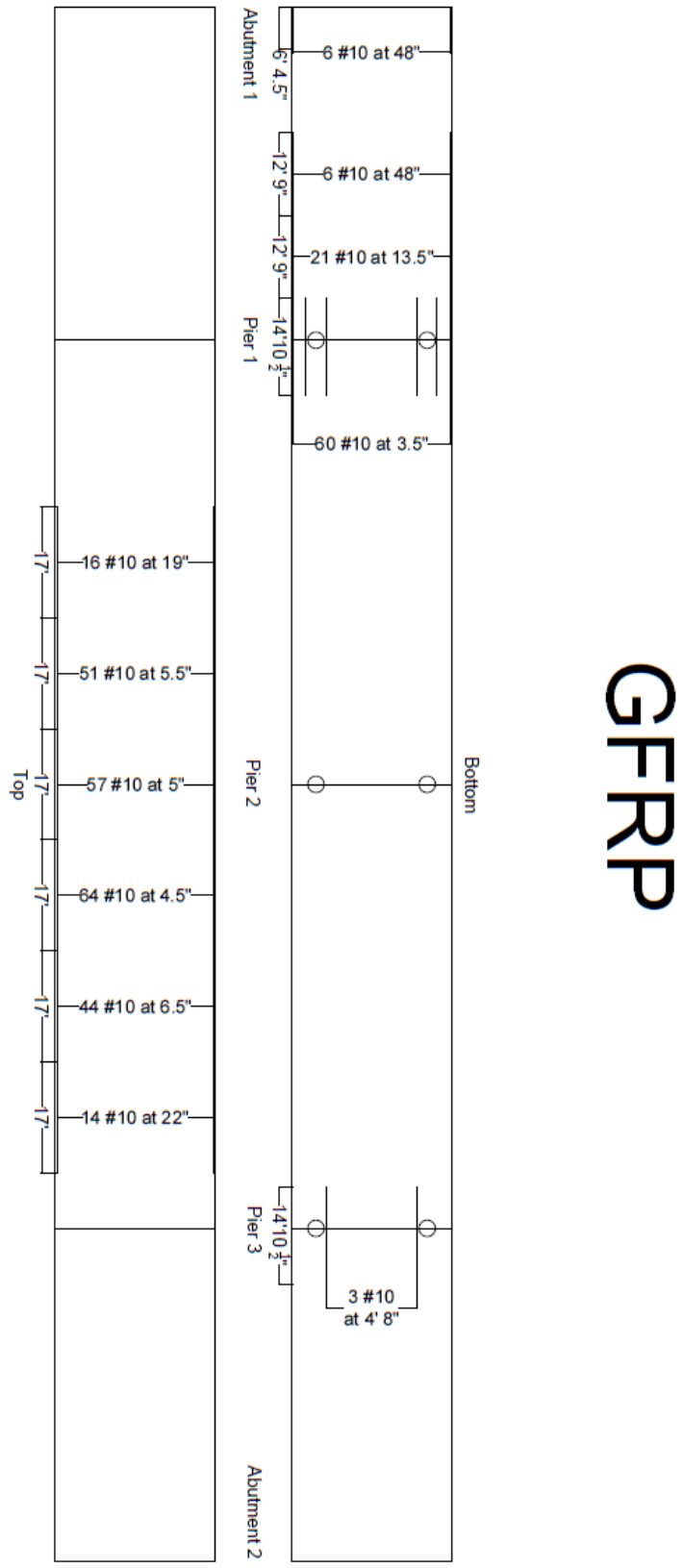

Figure 37: GFRP Span Layout

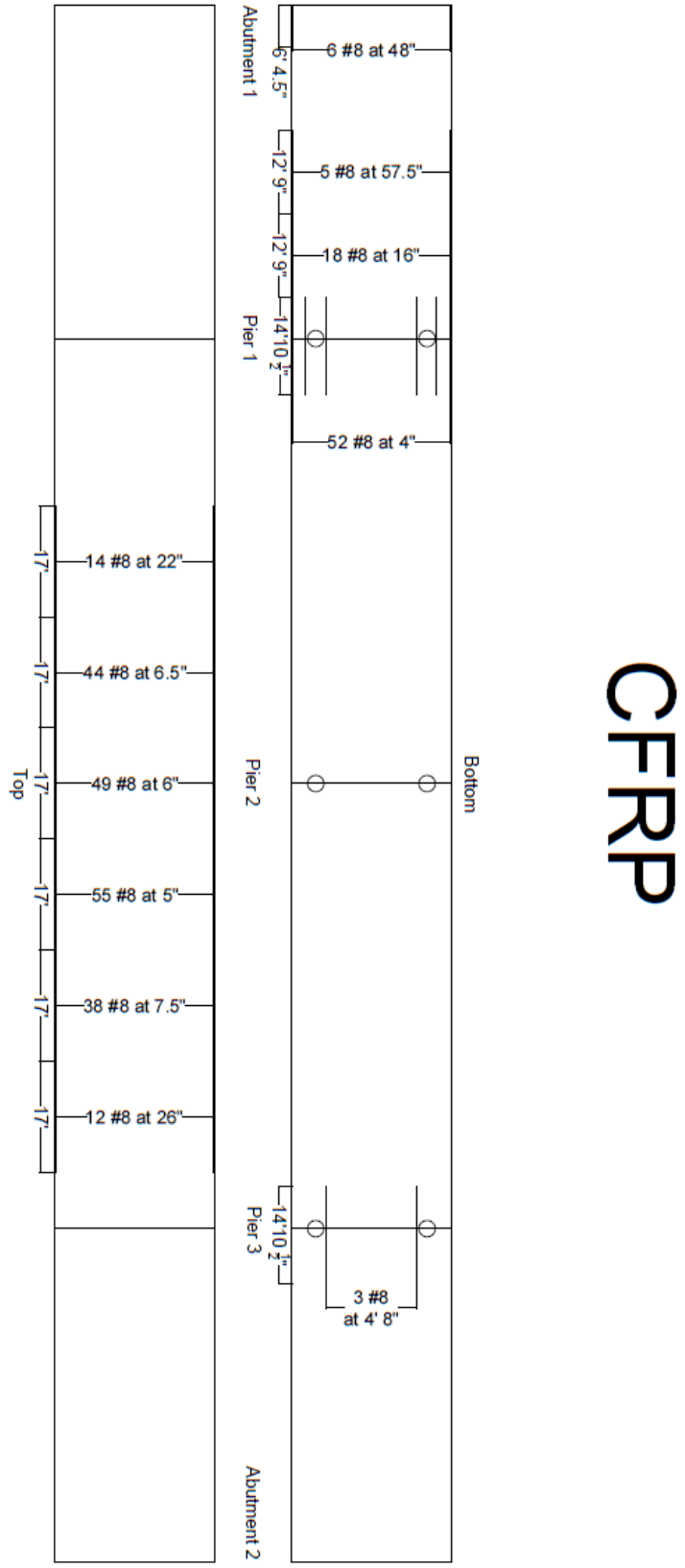

Figure 38: CFRP Span Layout

In order to account for ease of construction, a strengthening plan that used carbon fiber V-Wrap sheets was developed for the locations where bars were required to be installed on the bottom slab, underneath the bridge. The sheets will allow for easier installation, rather than having to cut grooves above the workers, the sheets will be epoxied on to the existing surface. The sheets will be installed along span 1 as well as pier 3. They will be attached to the box girder using anchors spaced at 2 feet in each direction. Figure 39 shows the layout as well as the number and dimensions of the sheets for the box girder. It is also recommended to use the V-Wrap sheets around the top of the piers. The wrapping would consist of a single sheet attached to the top two feet of each pier. This wrap would increase the strength of the piers by confining the concrete where the cracking is occurring on the bridge and the high stress concentration occurs in the Abaqus model.

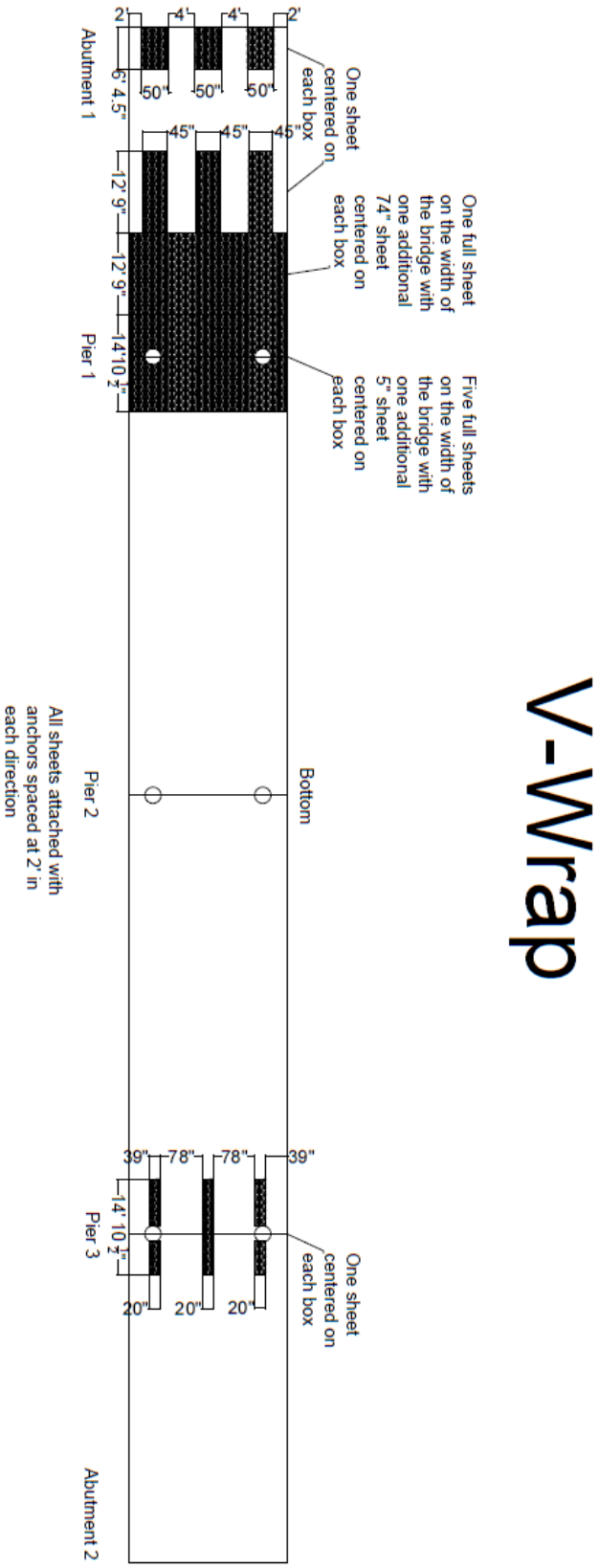

Figure 39: V-Wrap Layout

Conclusion

The following conclusions may be drawn from the present study:

1. The Abaqus analysis shows that the concrete maximum strength of 4 ksi is not exceeded in any component of the bridge except for the junction of the piers with the cross-beams under the April 2017 settlements. This is believed to be a stress concentration from the analysis. Tensile piles are not prone to pulling out.
2. The Abaqus analysis shows the same conclusions apply when the April 2017 settlements are combined with truck loading.
3. The RISA3D analysis shows that the top and bottom slabs of the box girder as well as one of the piers at the critical location exceed the sectional envelope as a tensile force under April 2017 settlements. The box girder web at critical locations exceed the sectional envelope as a pure bending moment. All piles are safe except one pile under the abutment 1, which slightly exceeds the sectional envelope.
4. The RISA3D analysis shows the same conclusions apply when the April 2017 settlements are combined with truck loading.
5. The RISA3D analysis shows the same conclusions apply when the April 2017 settlements are combined with projected settlements up to 2022.
6. Using a transformed I-Girder section (which is equivalent to the box girder section under axial force plus uniaxial bending moment) in addition to the RISA 3D analysis shows the transformed section fails in the same sections where the axial tension exceeded the capacity of the top and bottom slabs in the original analysis.
7. The addition of FRP rebar to top and bottom of the box girder can add strength to the transformed section in order to withstand future settlements.

References

Aggour, Sherif M., and Shafik M. Aggour. "Settlement of Simply Supported Bridge." *ASCE Journal of Structural Engineering* 112.8 (1986).

Armstrong, Amit, Roger Surdahl, and H. Gabriella Armstrong. "Peering into the Unknown." *Public Roads* (2009).

Bowles, Joseph E. *Foundation Analysis and Design.* Eds. B. J. Clark, Kiran V. Kimbell, and John M. Morris. 5th Edition ed.McGraw -Hill, 1996. 932-933 934.

Dedo, Darren. "KSN Investigates: The Money Pit." *KSN.com.* 2/4/2017 2017. Web. 2/7/2017 <http://ksn.com/2017/02/02/ksn-investigates-the-money-pit/>.

Gurbuz, Ayhan, and Samuel G. Paikowsky. "New Simple Approach to Prediction of Axial Settlement of Single Piles Under Design Load." *ASCE Journal of Bridge Engineering* (2016).

Halim, Abdul Halim, Asad Esmaeily, and Hayder A. Rasheed. "Behavior of RC Beams Under Combined Shear and Torsion According to AASHTO LRFD and ACI Equations." *The IES Journal Part A: Civil and Structural Engineering* 5.2 (2012): 95-105.

Lefchik, Thomas E., L. Rick Ruegsegger, and Robert W. Henthorne. "Avoiding Voids." *Public Roads* (2003).

O'Shea, Dennis M. "How could a Pile of Dirt Cause a Major Interstate Bridge to Tilt?" *Public Roads* (2015).

Rabbat, B. G., and H. G. Russell. "Friction coefficient of steel on concrete or grout." Journal of Structural Engineering 111.3 (1985): 505-515.

Wardle, Gavin. "Gold Mining from 1900 Presents Challenges for Road Construction." *Civil Engineering: Magazine of the South African Institution of Civil Engineering*. March/April 2001 (2001): 15-16.